LANGMUIR

pubs.acs.org/Langmuir Article

Moisture Retention and Multi-mechanistic Transport Behavior in Nanoporous Coal

Ang Liu, Shimin Liu,* and Kai Wang

Cite This: *Langmuir* 2022, 38, 14941−14958 Read Online

ACCESS | Metrics & More | Article Recommendations

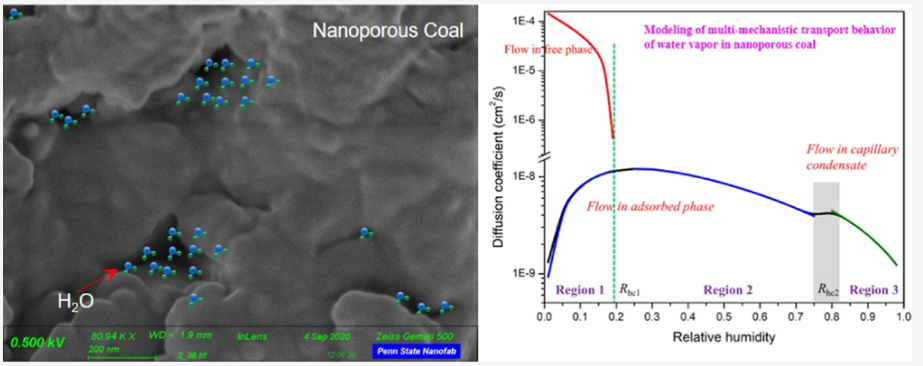

ABSTRACT: Coal−water interactions induced by water retention in coals control the performance of coalbed methane reservoirs and coal utilizations. Experimental measurements on Illinois coal samples using X-ray diffraction, X-ray photoelectron spectroscopy, Fourier transform infrared spectroscopy, low-temperature N_2 adsorption, low-pressure CO_2 adsorption, and dynamic water vapor sorption were carried out. A mechanism-based isothermal model of water vapor sorption was proposed to estimate the water adsorption capacity at varied relative humidity, which implicitly considered both monolayer and multilayer adsorptions and capillary condensation. The analytical models for quantifying the stage-based diffusion coefficients as well as the apparent diffusion coefficients at different relative humidities were proposed and well validated. The contributions of different diffusion regimes to the total mass flow were discussed. At the first stage, both free water vapor diffusion and surface diffusion of adsorbed water molecules contribute to the total mass flow whereas the apparent diffusion at this stage is dominated by latter flow regime; during the second stage, the contribution of free water vapor flow to the apparent flow can be neglected and the mass transfer at this stage is still dominated by the surface diffusion flow; upon reaching the critical relative humidity, the flow in capillary condensation will dominate the total mass flow.

1. INTRODUCTION

As a porous medium, coal does not only serve as a storehouse for gas but also provides the adsorbed site and storage volume for water in liquid/vapor/solid phases. Water can influence gas sorption behavior in both free and adsorbed phases, gas diffusivity, and relative permeability in the cleats/fractures.[1−7] Water naturally exists in coal formation and its interactions with coal generally include inherent moisture in the coal matrix, adsorbed water on the surface of the coal matrix, and free water in the fracture system.[6,8] Coal is organic matter-rich fossil fuel. The appearance of moisture in organic matter mainly promotes partial combustion and enhances smoke formation, whereby the evolution of heat is decreased. The adsorbed water on the surface of the coal matrix can affect moisture/gas diffusivity and cause coal swelling effects. The free water in the fracture system affects the water/gas flow through the degree of saturation and relative permeability. A few other studies addressed the effects of water on coal by determining sorption capacities of gases on moisture coals, apparent/relative permeability evolutions, matrix swelling effects, mechanical properties,[9,10] and many others.[6−8,11−15] However, the fundamental mechanisms of water−coal interactions, including both moisture retention and moisture diffusivity in coals have not been fully understood.

Behaviors of moisture retention and transport in coals are very complex. The general consensus is that the weak dispersive attractions between the organic carbon and water as well as the strong associative interactions among water

Received: October 4, 2022
Revised: November 3, 2022
Published: November 18, 2022

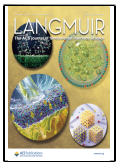

molecules are the main reasons.[16−19] The polar oxygen-containing groups including carboxyl, hydroxyl, and carbonyl provide the active sites are the main adsorption sites for primary adsorption through H-bonds formation. These oxygen-containing groups especially on the surfaces of the coal matrix and mineral matters can be treated as hydrophilic sites which provide the sorption sites for water molecules. Following the primary adsorption contributed by the monolayer adsorption, the multilayer adsorption and capillary condensation constituting the secondary adsorption can cause the formation of water clusters/pore fillings at relatively high relative humidity.[7,18,20−23] The isotherms of water vapor sorption, the combined effects of monolayer adsorption, multilayer adsorption, and capillary condensation were extensively studied.[16,24] For instance, the water vapor sorption isotherm typically shows the type II sorption shape with the increase of relative humidity based on IUPAC classification.[18,25] There are many other factors that have been identified to influence the shape of sorption isotherms such as the surface oxidation degree, mineral compositions, coal rank, pore volume, specified surface area, pore size distribution, and so on.[6,7]

To describe the sorption isotherm of water vapor, many classical models have been proposed.[26−30] The most popular model for describing the monolayer adsorption behavior is the Langmuir-type model.[28] However, the Langmuir-type sorption cannot be properly used to describe the entire curve of the moisture adsorption due to the presence of multilayer adsorption under relatively high relative humidities. The Brunauer−Emmett−Teller (BET) model has been widely used to quantify the sorption isotherms of moisture sorption.[26] The hypotheses behind the BET model include the lower binding energies exhibited at the secondary adsorption centers and the identical thermodynamic properties between the adsorbed water phase and the liquid water phase. However, the BET model fails to describe the water vapor sorption behavior at the relative humidity of 0.35 and beyond. Later, the BET model was improved and the best extension of which is the Guggenheim, Anderson, and De Boer model by adding an additional parameter comparing the potential of molecule clusters due to multilayer adsorption and the potential of liquid-phase water.[27,29,31] Many other semiempirical- and theoretical-based sorption models for describing water vapor sorption isotherms have been extensively proposed. Typically, the isotherm model of water vapor sorption has been continuously evolved and improved.[17,18,32−34]

Coal is classified as a dual-porosity porous medium with meso/micro/nano pores within the coal matrices and a developed cleat system.[35−40] In addition to the complex water retention behavior in nanoporous coal, kinetic characteristics of moisture transport are also very complex. Based on the diffusion mechanisms of fluids in porous medium, several mass transport mechanisms can be concluded as: (1) bulk diffusion controlled by the collisions among fluid molecules which dominates in relatively larger pore channels and under high-pressure condition; (2) Knudsen diffusion determined by the inter-collisions between the fluid molecules and the surface of flow pathways which is significant when the mean free path of the fluid molecule and the pore diameter is comparable; and (3) the surface diffusion driven by the concentration difference on the surface of solid matrix.[41,42] In addition, capillary condensation in coal induced by water vapor sorption under relatively high relative humidity is a unique phenomenon. Typically, the flow regimes of toluene in untreated Vycor glass with a pore radius of 3.1 nm and Vycor glass with a pore radius of 2.1 nm whose pores were artificially derivatized with $C_{18}H_{38}$ were theoretically and experimentally validated.[43] It has been proved that for both artificial and natural nanoporous materials, the wettability of nanoconfined water on these nanoporous materials dramatically causes the surface diffusion coefficients and effective viscosity for the flow in the capillary condensate substantially deviating from the bulk ones.[44−47] To our best knowledge, not enough materials reported on the apparent kinetic behavior of water vapor in coal. Therefore, it is necessary to model the mass transfer process of water vapor in coal, which lays foundations for better understanding of water transport in coal.

Two samples from Illinois Basin were collected and characterized in this study. The sorption isotherm model of water sorption in coal is proposed and validated against with the dynamic water vapor sorption data. Based on the experimental data, the mass transfer of water vapor in coal can be divided into three mechanisms including the flow of water vapor in the free phase, surface flow of water vapor in adsorbed phase with combined monolayer and multilayer adsorptions, and the flow in capillary condensate. Furthermore, we proposed a theoretical model to define the stage-based diffusion coefficients and an inclusive apparent diffusion coefficient was established and estimated over the entire range of relative humidity. The theoretical model is validated against with the apparent diffusion coefficients regressed from the unipore model and then the contributions of different flow regimes to the apparent diffusion coefficient were discussed. These results provide a rational method for analyzing the moisture retention and multi-mechanistic transport behaviors in coals.

2. MOISTURE RETENTION AND MULTI-MECHANISTIC TRANSPORT IN COALS

2.1. Sorption Isotherm of Water Vapor in Coal. To understand the stage-based behavior of water vapor sorption over the entire relative humidity range, the water vapor sorption should be segmented into different stages. As a prerequisite, the water vapor sorption isotherm curve should be precisely modeled. It is presumed that water molecules initially prefer to adsorb on the hydrophilic adsorption sites exhibiting monolayer distribution behavior. The strong binding energy between the oxygen-containing functional groups on the hydrophilic sites and the water molecules is responsible for the primary adsorption. With the continuous increase in the relative humidity, the occupied water molecules in monolayer behavior can provide the adsorption centers for multilayer adsorption, water cluster formations, and water condensation in nanoscale pores. However, there are no clear boundaries between the different stages. Before the full coverage of the monolayer adsorption, the multilayer adsorption can start at certain sites. Also, before the completion of multilayer adsorption stage, the capillary condensation is supposed to already begin to occur at a heterogeneous surface. For the sake of simplification of modeling, in this study, the primary adsorption is equivalent to the monolayer adsorption and the secondary adsorption accommodates both the multilayer adsorption and capillary condensation.

The monolayer adsorption model, Langmuir-type model, is commonly used and validated to explain the sorption mechanisms and behavior. The Langmuir-type sorption

https://doi.org/10.1021/acs.langmuir.2c02701
Langmuir 2022, 38, 14941−14958

model is appropriate to quantify the monomolecular coverage of the water vapor sorption process, which can be described as[28]

$$m_{pri} = \frac{m_L R_h}{R_L + R_h} \quad (1)$$

where m_{pri} is the primary adsorption capacity of water vapor at a given relative humidity, g/g; m_L is the maximum moisture retention capacity corresponding to a complete monolayer coverage, g/g; R_L is the relative humidity at which the measured moisture retention capacity is equal to $1/2m_L$, dimensionless; R_h is the given relative humidity, dimensionless, $R_h = \left.\frac{p_V}{p_{VS}}\right|_T$; p_V is the partial pressure of water vapor, kPa; p_{VS} is the pressure of saturated water vapor at specified temperature T, kPa; and T is the specified temperature, K.

To accommodate the multilayer adsorption and capillary condensation, the Dubinin−Serpinsky model can be used as[48]

$$m_{sec} = \frac{m_0 c k R_h}{1 - c k R_h} \quad (2)$$

where m_{sec} is the secondary adsorption capacity of water vapor at a given relative humidity, g/g; m_0 is the prioritized adsorption capacity for secondary adsorption, g/g; k represents the loss of the secondary sites in the course of adsorption, dimensionless, which can be treated as unity; and c is the ratio between the rate constants of adsorption and desorption, dimensionless.

It is presumed that all the adsorbed water molecules during the primary adsorption stage can provide the adsorption centers for the secondary adsorption and are available for the formation of water clusters during the water condensation stage. That is, the water molecules uptake on the hydrophilic sorption sites (m_0 in eq 2) can be regarded as the primary adsorption capacity of water vapor based on the Langmuir-type sorption model (m_{pri}) (eq 1). However, due to the mechanical constraints to pore structure, swelling, or steric effects, and other unknow effects, not all the water molecules during the primary adsorption stage can be considered as sorption sites for the secondary adsorption. Therefore, a parameter ω was introduced to define the non-perfectly multilayer formation building from the monomolecular coverage—the water vapor uptake on hydrophilic adsorption centers (m_0) can be calculated as $m_0 = \omega m_{pri}$, where $0 \leq \omega \leq 1$.[18] Therefore, the sorption isotherm model at a given relative humidity can be expressed as

$$m = m_{pri} + m_{sec} = \frac{m_L R_h (1 - c R_h + c\omega R_h)}{(R_L + R_h)(1 - c R_h)} \quad (3)$$

Equation 3 can be reduced to the generalized D'Arcy−Watt model if all the adsorbed molecules on primary centers can be treated as the sorption centers for secondary adsorption (ω = 1). It should be noted that the generalized D'Arcy−Watt model is equivalent with the the Guggenheim, Anderson, and De Boer model. Barton et al. found that only 17% of the water molecules' uptake on the hydrophilic sorption sites can be performed as the centers for secondary adsorption.[49] Also, other studies showed that water molecules' uptake on the hydrophilic sorption sites can form bonds for the formation of micro-clusters consisting of two to three molecules during the multilayer sorption stage.[50,51] Furmaniak et al. summarized that the range interval of ω is between 0 and 3 for carbonaceous materials.[18] ω is regarded as unity in this study. Therefore, eqs 1 and 2) are applied for representing the primary and secondary adsorption, respectively. Equation 3 combined both primary and secondary adsorptions by assuming that the primary adsorption sites can also be played as the secondary adsorption sites.

2.2. Quantifications of Mass Transfer Induced by Dynamic Flow Regimes. Many factors including pore properties (i.e., pore radius/width/volume, tortuosity, connectivity, etc.), coal properties (i.e., hydrophilicity, specific surface area, mineral components, etc.), water vapor properties (i.e., vapor pressure, viscosity, etc.) and other environmental conditions (i.e., temperature, external stress, etc.) will influence the mass transfer process of water vapor in coal. With relative humidity increasing, those factors will continuously vary and thereby the resultant flow regimes of water vapor in coal will experience dynamic variations. The total mass transfer at different stages over the entire relative humidity range is expected to be a multi-mechanism process with the mutual combinations of flow of water molecules in the vapor phase, surface flow of water molecules in the adsorbed phase that accommodates both monolayer and multilayer adsorption, and flow of capillary condensate.

2.2.1. Flow of Water Molecules in the Vapor Phase. For the flow of water molecules in the vapor phase in pore channels, the vapor pressures at exterior and interior of a pore channel determine the vapor pressure gradient. In addition to the driving forces on free water molecules caused by the vapor pressure gradient, the effective flow channel is the structural factor that can influence the transport behavior of free water molecules. Typically, the effective pore channel can be narrowed down due to the surface flow of water molecules in the adsorbed phase and flow of water molecules in capillary condensate. By neglecting the convective air flow effects, the isothermal steady-state flow of water molecules in the vapor phase can be described through an adaption of the vapor diffusion in free air[52]

$$q_V = -\frac{D_0 \phi (1 - S_w)\tau}{M} \nabla \rho_V \quad (4)$$

where q_V is the vapor flux of water molecules in the vapor phase, mol/(cm^2•s); D_0 is the diffusion coefficient of free water vapor in air, cm^2/s;ϕ is the porosity of the porous medium, dimensionless; τ is the tortuosity of the porous medium, dimensionless; M is the water molar mass, g/mol; ρ_V is the mass density of water vapor in the free phase, g/cm^3, where $\rho_V = R_h \rho_{VS}$ based on the definition of relative humidity (ρ_{VS} is the mass density of saturated water vapor under a given temperature, g/cm^3 and thus ρ_V should be spatially related to R_h under a given temperature); and S_w is the water saturation, cm^3/cm^3, which is defined as the ratio of water volume to the total pore volume. Based on the definition, water saturation ranges between 0 and 1. The value of "0" represents the fully dry condition and the value of "1" indicates the fully saturated condition in pores. By assuming water molecules only occupy the pore space, the water saturation can be calculated from $S_w = \frac{V_w}{V_p} = \frac{m_t m_c}{\rho_{lw} V_c \phi m_c} = \frac{\rho_c}{\rho_{lw}\phi} m$, where V_w, V_p, and V_c are water, pore, and total coal volumes, respectively, cm^3; m_t and m_c are water and coal masses, respectively, g; and ρ_c and ρ_{lw} are mass densities of coal and liquid water, respectively, g/cm^3. The physical significance of the term "$(1 - S_w)$" in eq 4 represents

https://doi.org/10.1021/acs.langmuir.2c02701
Langmuir 2022, 38, 14941−14958

the effective pore channel space that are still available for flow of water molecules in the vapor phase. Typically, the effective pore channel space can be narrowed down due to the surface flow of water molecules in the adsorbed phase and flow of water molecules in capillary condensate. In other words, the initial difference of R_h values between the entrance of a pore and inside the pore initiates the flow of free water vapor molecules. When the free water vapor molecules occupies the whole pore region, the flow of free water vapor molecules will ease due to the disappeared R_h difference whereas the surface flow of water molecules in the adsorbed phase and flow in capillary condensate under the spreading pressures will not terminate and thus the water saturation (S_w) can be more.

By simplifying eq 4, the vapor flux of water molecules in the vapor phase can be expressed in terms of the relative humidity gradient

$$q_V = -\frac{\rho_{VS} D_0 \phi (1 - S_w)\tau}{M} \nabla R_h \tag{5}$$

At each relative humidity stage, the environmental relative humidity outside the coal particle is constant, whereas the difference of relative humidity at the inlet and outlet of the coal particle induces the concentration gradient as represented in eqs 4 and 5. We used the transient water vapor sorption data at each relative humidity stage to fit the average diffusion coefficient along the whole equilibrium time period in Section 2.4.

By recalling the classical Fick's law[53]

$$q = -D\nabla C \tag{6}$$

where q is the flow flux induced by diffusion, mol/(cm^2·s); D represents the diffusion coefficient, cm^2/s; and C is the fluid concentration, mol/cm^3. For the flow of water molecules in the vapor phase in coal, the concentration of water vapor in the free phase can be expressed based on the Equation of State

$$C_V = \frac{n_V}{V_p} = \frac{p_v}{ZRT} = \frac{p_{vs}}{ZRT} R_h \tag{7}$$

where C_V is the concentration of water vapor in the free phase, mol/cm^3; n_V is the molar amount of water vapor molecules in the free phase, mol; R is the universal gas constant, J/(mol·K); and Z is the compressibility factor of water vapor, dimensionless.

Based on eqs 5−7, the diffusion coefficient of water molecules in the vapor phase can be expressed as

$$D_V = \frac{\rho_{VS} D_0 \tau ZRT \phi (1 - S_w)}{M p_{vs}} \tag{8}$$

where D_V represents the diffusion coefficient of water molecules in the vapor phase, cm^2/s.

2.2.2. Surface Flow of Water Molecules in the Adsorbed Phase. In addition to flow of water molecules in the free vapor phase, surface flow of water molecules adsorbed on the surface of the solid wall can also take place.[43] Surface flow can be described by the hopping model, the random walk model, or the hydrodynamic model.[54] Typically, the hydrodynamic model assumes that the adsorbed phase can be regarded as a liquid film which can slide along the surface driven by the pressure gradient. To quantify the surface flow of water molecules in the adsorbed phase, the dynamical equation of motion was first analyzed.

To develop the dynamical equation of motion, a volume element of fluid will generally be subjected to three types of forces including the pressure gradient in the form of ∇P; the viscous force acting on a unit volume arising from the velocity gradients within the fluid written in the form of ψ; and the external "body force" written in the form of F acting on a unit volume of the fluid, such as gravity.[55] By equating these forces to the product of the mass and acceleration of the volume element, the generalized equation of motion for a volume element of fluid can be expressed as[55]

$$\rho \frac{Du}{Dt} = -\nabla P + \psi + F \tag{9}$$

where D/Dt represents a differentiation following the motion of the fluid; ρ is the mass density of fluid, g/cm^3; u is the fluid velocity, cm/s; ∇P is the pressure gradient, g/(cm^2·s^2); F is the external force of a volume element, g/(cm^2·s^2); and ψ is the viscous resisting force acting on a unit volume arising from the velocity gradients within the fluid, g/(cm^2·s^2). Because the velocity of surface flow caused by the movement of water molecules in the adsorbed phase is extremely small, the accelerative force will be negligible compared to other forces and thus the left term in eq 9 can be regarded as zero. Due to the negligible mass of water vapor, the gravitational force can also be neglected, that is, $F = 0$. With the low velocity of water molecules in the adsorbed phase, it is presumed that the viscous resisting force acting on a unit volume arising from the velocity gradients within the fluid is linear with the velocity (u), which can be expressed using Darcy's law[56]

$$\psi = -\alpha \mu u \tag{10}$$

where α is the coefficient of viscous flow resistance, 1/cm^2 and μ is the fluid viscosity, Pa·s.

Based on the hydrodynamic model, the pressure arising from the solid−fluid interface leads to the movement of the liquid film of water molecules in the adsorbed phase with the velocity of u. It is presumed that the pressure acting on a unit volume can be calculated from the spreading pressure p_s, which can be expressed as[55]

$$P = p_s A = nRT \ln \frac{n}{n - n_s} \tag{11}$$

where p_s is the spreading pressure, N/cm, which is as a function of the free energy of the liquid film constituting the water molecules in the adsorbed phase; A is the surface area per unit volume, cm^2/cm^3; n is the maximum number concentration of primary adsorption sites, mol/cm^3; and n_s is the actual number concentration of water molecules adsorbed on primary adsorption sites, mol/cm^3.

Substituting eqs 10 and 11 into eq 9, neglecting the accelerative force ($\rho Du/Dt = 0$) and the external forces ($F = 0$), it can be arrived at

$$u_a = -\frac{nRT}{\alpha \mu} \nabla \left(\ln \frac{n}{n - n_s} \right) \tag{12}$$

where u_a is the flow velocity of water molecules in the adsorbed phase, cm/s.

Subsequently, the surface flow flux of water molecules in the adsorbed phase can be derived as

$$q_a = n_t u_a = -\frac{n_t RT}{\alpha \mu} \frac{n}{n - n_s} \nabla n_s \tag{13}$$

https://doi.org/10.1021/acs.langmuir.2c02701
Langmuir 2022, 38, 14941−14958

where q_a is the surface flow flux of water molecules in the adsorbed phase, mol/(cm^2·s) and n_t is the total number concentration of water molecules adsorbed at primary and secondary adsorption stages, mol/cm^3, as quantified in eq 3. Based on eq 3, the relation between the total number concentration of adsorbed water molecules (n_t) and the maximum number concentration of primary adsorption sites (n) can be expressed as

$$\frac{n_t}{n} = \frac{R_h}{(R_L + R_h)(1 - cR_h)} \tag{14}$$

Similarly, the relation between the actual number concentration of water molecules adsorbed on primary adsorption sites (n_s) and the maximum number concentration of primary adsorption sites (n) can be expressed by

$$\frac{n_s}{n} = \frac{R_h}{R_L + R_h} \tag{15}$$

By substituting eqs 14 and 15 into eq 13, it gives

$$q_a = -\frac{n^2 RT}{\alpha\mu} \frac{R_h}{(R_L + R_h)^2(1 - cR_h)} \nabla R_h \tag{16}$$

The concentration of water molecules in the adsorbed phase can be expressed as

$$C_a = \frac{N_t}{V_p} = \frac{m_t}{M}\frac{m_c}{m_c V_p} = \frac{m_t}{M m_c}\frac{\rho_c V_c}{V_p} = \frac{\rho_c}{\phi M}\frac{m_L R_h}{(R_L + R_h)(1 - cR_h)} \tag{17}$$

where N_t is the total number of adsorbed water molecules, mol. It should be noted that m_t/m_c is the gravimetric water content m, g/g, as defined in eq 3.

Based on eqs 6, 16, and 17, the diffusion coefficient of water molecules in the adsorbed phase can be calculated as

$$D_a = \frac{n^2 RTR_h \phi M(1 - cR_h)}{\alpha\mu\rho_c m_L (R_L + cR_h^2)} \tag{18}$$

where D_a represents the diffusion coefficient of water molecules in the adsorbed phase, cm^2/s.

2.2.3. Flow of Water Molecules in the Capillary Condensate Phase. So far, a broad consensus has been reached that the Kelvin equation remains accurate for meniscus curvature with a diameter larger than 8 nm and can also describe condensation phenomena in hydrophilic pores as small as 4 nm in diameter.[57] In this study, van der Waals assembly of two-dimensional crystals was used to create atomic-scale capillaries and study condensation within them. Their smallest capillaries are less than 4 Å (0.4 nm) in height and can accommodate just a monolayer of water. Surprisingly, even at this scale, it was found that the macroscopic Kelvin equation using the characteristics of bulk water describes the condensation transition accurately in strongly hydrophilic (mica) capillaries and remains qualitatively valid for weakly hydrophilic (graphite) ones.[57] Therefore, the Kelvin equation is certainly enough to evaluate the critical relative humidity for coals.

For the flow of water molecules in the capillary condensate phase, the capillary pressure will be the driving force for the movement. The capillary pressure for flow in capillary condensate based on the Kelvin−Laplace law can be expressed as[58]

$$p_c = \frac{\rho_{lw} RT}{M} \ln R_h = -\frac{\gamma}{\mathcal{R}(h)} \tag{19}$$

where p_c is the capillary pressure of water molecules in the capillary condensate phase, Pa; γ is the surface tension coefficient, N/cm; and $\mathcal{R}(h)$ is the radius of curvature of the capillary interface, nm.

Still, by assuming that the external forces (i.e., F) and the accelerative force (i.e., $\rho Du/Dt$) are negligible in the dynamical equation of motion (eq 9, and substituting eqs 10 and 19 into eq 9, it rearranges and yields

$$u_c = \frac{\rho_{lw} RT}{\alpha\mu M R_h} \nabla R_h \tag{20}$$

where u_c is the flow velocity of water molecules in the capillary condensate phase, cm/s.

The flow flux of water molecules in the capillary condensate phase can be expressed as

$$q_c = n_t u_c = -\frac{n\rho_{lq} RT}{\alpha\mu M} \frac{1}{(R_L + R_h)(1 - cR_h)} \nabla R_h \tag{21}$$

where q_c is flow flux of water molecules in the capillary condensate phase, mol/(cm^2•s).

Based on eqs 6, 17, and 21, the diffusion coefficient of water molecules in the capillary condensate phase can be expressed as

$$D_c = \frac{n\phi\rho_L RT(R_L + R_h)(1 - cR_h)}{\alpha\mu\rho_c m_L (R_L + cR_h^2)} \tag{22}$$

where D_c represents the diffusion coefficient of water molecules in the capillary condensate phase, cm^2/s.

2.3. Apparent Diffusion Coefficient of Water Vapor Transport in Nanoporous Coal. As quantified in eqs 8, 18, and 22, the diffusion coefficients of water molecules in the vapor phase, the adsorbed phase, and the capillary condensate phase were derived. Thus, the apparent diffusion coefficient of water vapor transfer in coal should be a function of these three individual diffusion coefficients. To divide the apparent diffusion coefficient into different stages, it is a prerequisite to find the turning point, that is, the starting point of the formation of capillary condensation. At a given temperature, the radius of curvature of a capillary interface ($\mathcal{R}(h)$) is a function of the relative humidity of the gaseous phase whereas the thickness of the adsorbed layer ($t(h)$) is also a function of the relative humidity. Based on the assumption that capillary condensate filling of a pore occurs only when the coaxial cylindrical meniscus of the adsorbed layer reaches the radius of curvature given by Kelvin−Laplace law, for a given relative humidity, the criteria for evaluating the pores where the capillary condensation takes place can be expressed as[58]

$$r_p - t(h) < R(h) \tag{23}$$

where r_p is pore radius, nm and $t(h)$ is the thickness of the adsorbed layer, nm. Equation 23 illustrates that the pores where capillary condensation occurs are those with radius small enough to allow a spherical meniscus to form. For a given value of R_h, the total volumetric water content (S_V) involving capillary and adsorbed water can be expressed as

https://doi.org/10.1021/acs.langmuir.2c02701
Langmuir 2022, 38, 14941−14958

$$S_V = \eta[\mathcal{R}(h) + t(h)] + t(h)\cdot S[\mathcal{R}(h) + t(h)] \quad (24)$$

where $\eta(r_p)$ is the volume fraction of pores with radii smaller than r_p, dimensionless and $S(r_p)$ is the area of pores with radii larger than r_p, cm^2/cm^3.

Based on eq 19, it is shown that there are no pores smaller enough to allow capillary condensation for small R_h. That is, there is a range of $R_h < R_{hc}$ in which only surface adsorption occurs. By neglecting the capillary condensation, the domain with only adsorption process can be written as

$$S_V = t(h)\cdot S(0) \quad (25)$$

where $S(0)$ is the total area of pores per unit volume, cm^2/cm^3 and R_{hc} is the critical relative humidity for capillary condensation, dimensionless.

By recalling eq 19, a relation between the volumetric water content S_V and the capillary pressure (p_c) can be used to evaluate the critical relative humidity, which can be expressed as[59]

$$\ln|p_c| = a - bS_V = a - bt(h)\cdot S(0) \quad (26)$$

where a and b are the regression parameters from experimental data. Equation 26 holds only for adsorption stage without capillary condensation.[58] Thus, the threshold R_{hc} can be roughly estimated from the linear relation. Based on eqs 25 and 26, the value of the function $t(h)$ before the critical relative humidity can be determined as

$$t(h) = \frac{a - \ln|p_c|}{bS(0)} \quad (27)$$

Under low values of relative humidity, the flow of water vapor in the free phase and the flow of water vapor in the adsorbed phase dynamically contribute to the total mass flow depending on the relative humidity. It is necessary to give the weighting factors for the two flow regimes. For a representative element volume, the contents of water molecules in free and adsorbed phases in coal can be quantified as

$$m_f = \phi(1 - S_w)\frac{p_{vs}M}{ZRT}R_h \quad (28)$$

$$m_{ad} = [1 - \phi(1 - S_w)]\frac{\rho_c m_L R_h}{(R_L + R_h)(1 - cR_h)} \quad (29)$$

where m_f is the content of water molecules in the vapor phase, g/cm^3 and m_{ad} is the content of water molecules in the adsorbed phase, g/cm^3.

Based on eqs 7, 17, 28, and 29, the mass flow flux of water molecules in a representative element volume can be expressed as

$$q_t = q_V + q_a = -D_V\nabla C_V - D_a\nabla C_a = -\frac{D_V}{M}\nabla m_f - \frac{D_a}{M}\nabla m_{ad} \quad (30)$$

where q_t is total mass flux, $mol/(cm^2\cdot s)$; q_V and q_a are the flow fluxes of water molecules in the free vapor phase and the adsorbed phase, respectively, $mol/(cm^2\cdot s)$. In eq 30, the adsorbed phase and the free vapor phase were considered as the two contributions to the total flow flux. The contribution of the transition phase from the free phase to the adsorbed phase was not considered here.

Based on eqs 28 and 29, the following weighting factors can be defined

$$f_V = \frac{m_f}{m_f + m_{ad}} = \frac{\phi(1 - S_w)\frac{p_{vs}M}{ZRT}R_h}{\phi(1 - S_w)\frac{p_{vs}M}{ZRT}R_h + [1 - \phi(1 - S_w)]\frac{\rho_c m_L R_h}{(R_L + R_h)(1 - cR_h)}} \quad (31)$$

$$f_{ad} = \frac{m_{ad}}{m_f + m_{ad}} = \frac{[1 - \phi(1 - S_w)]\frac{\rho_c m_L R_h}{(R_L + R_h)(1 - cR_h)}}{\phi(1 - S_w)\frac{p_{vs}M}{ZRT}R_h + [1 - \phi(1 - S_w)]\frac{\rho_c m_L R_h}{(R_L + R_h)(1 - cR_h)}} \quad (32)$$

where f_V and f_{ad} are the weighting factors for flow flux in the free vapor phase and the adsorbed phase, respectively, dimensionless.

By introducing eqs 31 and 32 into eq 30, it yields

$$q_t = -\left(\frac{D_V}{M}f_V + \frac{D_a}{M}f_{ad}\right)\nabla\left(\frac{m_f + m_{ad}}{M}\right) = -(D_V f_V + D_a f_{ad})\nabla C_t \quad (33)$$

where C_t is the total concentration of water molecules in free and adsorbed phases, mol/cm^3.

Based on eqs 6 and 33, the apparent diffusion coefficient for the first stage below the critical relative humidity can be calculated as

$$D_{af} = D_V f_V + D_a f_{ad} = f_V\frac{\rho_{VS}D_0\tau ZRT\phi(1 - S_w)}{Mp_{vs}} + f_{ad}\frac{n^2RTR_h\phi M(1 - cR_h)}{\alpha\mu\rho_c m_L(R_L + cR_h^2)} \quad (34)$$

where D_{af} is the apparent diffusion coefficient during the first stage below the critical relative humidity, cm^2/s.

In this study, it is presumed that only flow in capillary condensate dominates the second stage. Based on eqs 22 and 34, the apparent diffusion coefficient over the entire relative humidity range can be expressed as

$$D_w = \begin{cases} f_V\frac{\rho_{VS}D_0\tau ZRT\phi(1 - S_w)}{Mp_{vs}} + f_{ad}\frac{n^2RTR_h\phi M(1 - cR_h)}{\alpha\mu\rho_c m_L(R_L + cR_h^2)}, & R_h < R_{hc} \\ \frac{n\phi\rho_L RT(R_L + R_h)(1 - cR_h)}{\alpha\mu\rho_c m_L(R_L + cR_h^2)}, & R_h \geq R_{hc} \end{cases} \quad (35)$$

where D_w is the apparent diffusion coefficient over the entire relative humidity range, cm^2/s, which is a continuous function of relative humidity and in which the critical relative humidity is a turning point. It should be noted that the water vapor molecules can also adsorb on the exterior surface of coal, instead of solely occupying the pore space, which may result in a negative value of term "$1 - S_w$" based on the expression of

https://doi.org/10.1021/acs.langmuir.2c02701
Langmuir 2022, 38, 14941−14958

Table 1. Proximate and Ultimate Analyses on Two Coal Samples (wt %)

	proximate analysis (as received)				ultimate analysis (air-dried basis)				
	fixed carbon	volatile	moisture	ash	C	H	O	N	S
IS #5	47.47	36.83	3.41	12.29	61.05	5.44	11.95	0.54	8.30
IS #6	52.40	33.92	3.59	10.09	67.83	5.07	12.83	0.74	3.06

Table 2. Mineralogical Composition Based on XRD Analysis (wt %)

sample	TOC	kaolinite	illite	szomolnokite	pyrite	quartz	calcite	anhydrite
IS #5	90.8	1.2		5.2	1.6	1.2		
IS #6	88.9	1.9	4.9	1.7	0.2	1.4	0.5	0.5

Table 3. Oxygen-to-Carbon Atomic Ratio (O/C) Based on XPS Analysis (%)

sample	Sp2 (aromatic carbon)	Sp3 (aliphatic carbon)	C−OH (hydroxyl)	C−O−C (epoxy)	C═O (carbonyl)	O−C═O (carboxyl)	O/C
	284.4 ev	285.0 ev	285.7 ev	286.7 ev	288.0 ev	290.1 ev	
IS #5	55.03	24.23	8.99	9.39	0	2.37	0.12
IS #6	56.55	9.37	13.32	11.09	7.50	2.17	0.18

$S_w = \frac{\rho_c}{\rho_{lw}\phi}m$ under an ideal assumption. In this study, we assume the flow of free water vapor will stop when the values of term "$1 - S_w$" reaches zero. Therefore, the contribution of the flow of water molecules in the free phase to the total flow will not be accounted into eq 35 when encountering with the negative value of term "$1 - S_w$".

2.4. Estimation of Diffusion Coefficient Based on the Unipore Model. The kinetic data of water vapor flow could be described by various models including the linear driving force mass transfer model, the unipore model, and the bidisperse model. Water diffusion coefficient in coal can be estimated from the unipore diffusion model, which is derived from Fick's second law of diffusion based on a few assumptions: (1) coal particles are homogeneous, isotropic, and spherically symmetric with uniform pores and (2) the adsorbate concentration at the surface of the spheres is constant. The Fick's diffusion equation in spherical coordinates takes the following form[60]

$$\frac{\partial C}{\partial t} = \frac{1}{r^2}\frac{\partial}{\partial r}\left(Dr^2\frac{\partial C}{\partial r}\right) = D\left(\frac{2}{r}\frac{\partial C}{\partial r} + \frac{\partial^2 C}{\partial r^2}\right) \quad (36)$$

where C and D are the adsorbate concentration and constant diffusion coefficient, respectively, mol/cm^3 and cm^2/s; and r is the particle radius, cm. Given a constant concentration at the surface of the spherical particle (constant concentration at the surface of the spherical coal particle is due to the constant relative humidity at each stage), the solution of eq 36 has the following form[61]

$$\frac{M_t}{M_\infty} = 1 - \frac{6}{\pi^2}\sum_{i=1}^{\infty}\frac{1}{i^2}\exp\left(-\frac{Di^2\pi^2 t}{r^2}\right) \quad (37)$$

where M_t is the accumulated amount of water adsorbed at time t before its equilibrium state of each relative humidity and M_∞ is the accumulated amount of water adsorbed at the final equilibrium state of each relative humidity state. Based on eq 37, under initial dry conditions (~0% R_H), the residual water desorbs and mass of the sample decreases to a constant value which is considered as the mass of the dry sample (or reference mass). Then, water vapor ad-/de-sorption isotherms for the studied coal samples can be calculated by taking the difference between the reference mass and the equilibrium mass of coal samples at a given relative humidity. Based on eq 37, we develop a MATLAB-based computer program based on a least-squares criterion to regress the experimental gas sorption kinetic data and determine the corresponding diffusion coefficient. The apparent diffusivity was adjusted using the Golden Section Search algorithm until the global minimum of the objective function was reached. Based on our practice, an entry of 50 for the summation is good enough to truncate the infinite summation. In this study, we used an entry of 100 for the summation. The detail information about the program can be found in our previous publication.[62] At each relative humidity stage, the diffusion coefficient dynamically changes with time before its equilibrium state, the average diffusion coefficient at each relative humidity is calculated and analyzed.

3. EXPERIMENTAL WORK

3.1. Sample Collection and Preparation and Characterization. Two sub-bituminous coal samples from Illinois Basin [Illinois sample #5 (IS #5) and Illinois sample #6(IS #6)] were collected and prepared in the laboratory. Prior to starting the actual tests, the prepared samples were kept in an environmental chamber under controlled conditions of temperature and humidity. Both the raw bulk coal samples were hand-pulverized and sieved to powders with sizes between 60−80 mesh. Coal powders were used to conduct the proximate/ultimate analysis, X-ray diffraction analysis (XRD), X-ray photoelectron spectroscopy (XPS) analysis, Fourier transform infrared spectroscopy (FTIR) analysis, low-pressure carbon dioxide adsorption (LPCDA) test, low-temperature liquid nitrogen adsorption (LTNA) test, and dynamic water vapor sorption measurement.

3.2. Sample Characterizations. *3.2.1. Proximate and Ultimate Analyses on Two Coal Samples.* Proximate and ultimate analyses on two coal samples were conducted with the results summarized in Table 1. The contents of fixed carbon, volatile, moisture, and ash are very close in both two coal samples IS #5 and IS #6 based on the proximate analysis. The elemental contents of carbon and oxygen in coal sample IS #6 are slightly higher than that in coal sample IS #5 whereas the sulfur content in coal sample IS #5 is ~2.71 times higher than coal sample IS #6.

3.2.2. Mineralogical Compositions in Two Coal Samples. The mineralogical compositions of two coal samples were analyzed by XRD and as summarized in Table 2, the total organic carbon (TOC) contents in two coal samples are ~90.8% (IS #5) and ~88.9 (IS #6), respectively. IS #6 contains clay minerals kaolinite (~1.9%) and illite (~4.9%), whereas IS#5 only contains ~1.2% of kaolinite. Other mineral contents are summarized in Table 2.

https://doi.org/10.1021/acs.langmuir.2c02701
Langmuir 2022, 38, 14941−14958

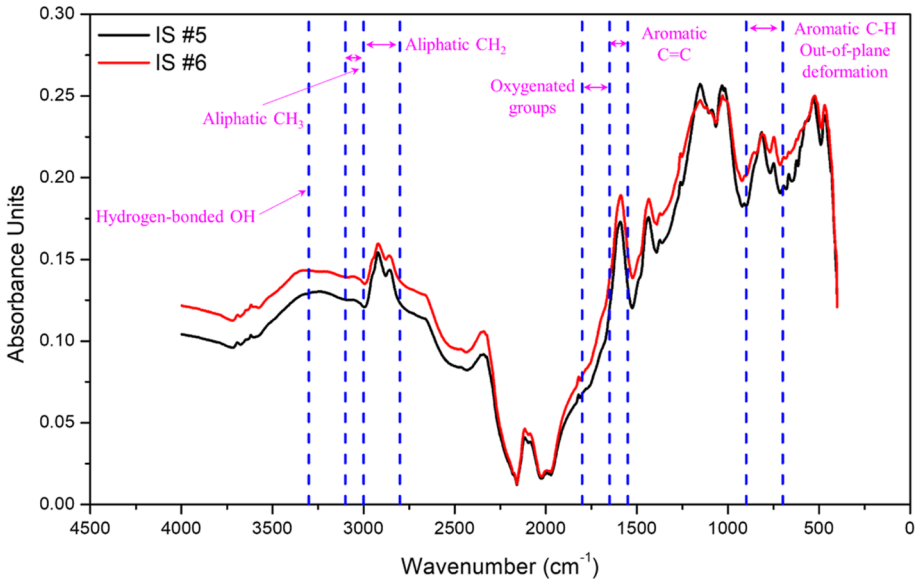

Figure 1. FTIR spectra of two coal samples.

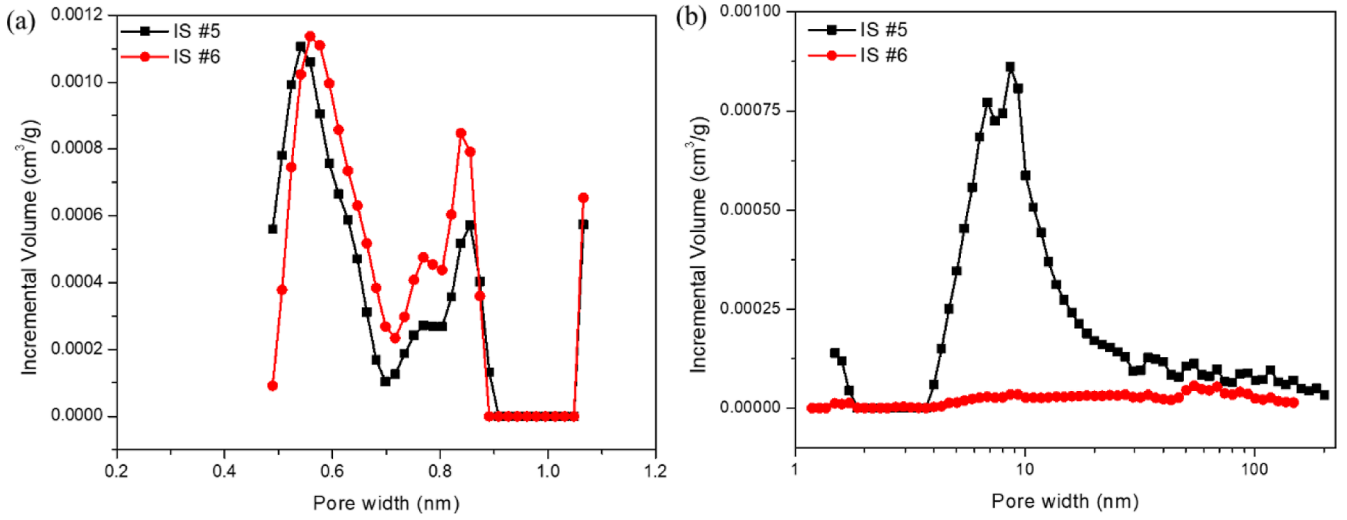

Figure 2. Pore size distributions based on DFT using (a) LPCDA test and (b) LTNA test.

3.2.3. XPS and FTIR Characteristics of Two Coal Samples. XPS technique allows a measure of surface oxygen-containing degree through the O/C ratio, which helps quantifying the different types of carbon functionalities present. The oxygen-containing degree indicates the formation of chemical bonds and evaluates the physisorption of molecules. Based on the deconvolution of the C 1s signal into its various contributions: graphitic carbon (sp2), defects (mainly sp3 carbon), carbons bonded to hydroxyl and epoxy groups, and those from carbonyl and carboxyl groups (Table 3). The symmetrical fitting of the O/C ratio is then calculated using these C 1s signals. The XPS results show that IS #6 has a little higher oxygen-to-carbon ratio (~0.18) than that of IS #5 (~0.12), which implicitly reflects that the oxygen-containing functional groups in IS #6 are richer than IS #5 and thus the hydrophilic properties of IS #6 should be more obvious than that of IS #5.

XPS technique can only acquire the information from the surface layers of coal powers. FTIR spectroscopy, as a nondestructive technique, offers the capacity of identifying functional groups in the bulk phase. For coals, the absorbance intensities of the FTIR spectra in the region of 1650−1800 cm^{-1} is assigned to oxygenated groups, 550−1650 cm^{-1} region assigned to aromatic C═C ring stretching, 2800−3000 cm^{-1} region assigned to aliphatic CH_2 stretching, 3000−3100 cm^{-1} region assigned to aliphatic CH_3 stretching, and 3300 cm^{-1}band assigned to hydrogen-bonded OH.[63]Figure 1 shows FTIR spectra of two coal samples. In the region of 1650−1800 cm^{-1} that is assigned to oxygenated groups, the absorbance intensities of FTIR spectra on coal IS #6 are slightly higher than that on coal IS #5. It confirms that coal IS #6 is more oxidized than coal IS #5, which is in agreement with the XPS results in Table 3.

3.2.4. Pore Size Distributions in Two Coal Samples. It is widely accepted that the LPCDA test, the LTNA test, and the high-pressure mercury injection can characterize the micropores (<2 nm), mesopores (2−100 nm), and macropores (>100 nm), respectively.[64] Based on the Kelvin−Laplace equation, capillary condensation primarily takes place in nanoscale pores with several nanometers and we therefore conducted both LPCDA and LTNA tests to obtain the pore size distributions of our coal samples using the Accelerated Surface Area and Porosimetry System 2420 (Micromeritics Instrument Corp). Typically, the adsorption/desorption measurements using the LTNA method were measured at 77.350 K, and CO_2 adsorption measurements were measured at 273.150 K. The pore size distributions were analyzed based on DFT.[65]

Figure 2 shows the pore size distributions (PSD) of coal samples IS #5 and IS #6, which were measured using the LPCDA test (Figure 2a) and the LTNA test (Figure 2b), respectively. In Figure 2a, the PSDs showed the micropores with pore widths less than 2 nm. For

https://doi.org/10.1021/acs.langmuir.2c02701
Langmuir 2022, 38, 14941−14958

samples IS #5 and IS #6, PSDs exhibit very similar trend, whereas the curve shifted a little bit to a smaller pore width in sample IS #5. The incremental pore volumes determined by the micropores for sample IS #6 is slightly higher than sample IS #5. As shown in Figure 2b, the mesopores in samples IS #5 and IS #6 showed significant differences and an obvious increase in the incremental pore volumes were observed in sample IS #5. By comparing with Figure 2a,b, the micro-scale pores are more developed in sample IS#5 whereas the pore volumes cumulated from micro to mesopores is higher in sample IS #5 mainly because of its developed mesopores.

3.3. Dynamic Vapor Sorption Measurement. The dynamic vapor sorption (DVS) intrinsic can accurately measure the mass changes of microgram samples as it sorbs precisely controlled concentrations of water vapors in a nitrogen carrier gas. The detailed description of the instrument is provided in our previous publication.[66] The water vapor sorption tests on coal samples IS #5 and IS #6 were measured at 30 °C. Each sample was measured three times for obtaining reliable data. For sample IS #5, they were notated as IS #5_ Test 1, IS #5_ Test 2, IS #5_ Test 3, and they were notated as IS #6_ Test 1, IS #6_ Test 2, and IS #6_ Test 3 for sample IS #6, respectively. One DVS test accommodates the elevated relative humidity values increasing from 0.1 to 0.98. As an example, the raw DVS data collected for IS #6 from Test 1 (IS #6_Test 1) are plotted in Figure 3. Under the initial dry condition ($R_h \sim 0$) in Figure 3, the

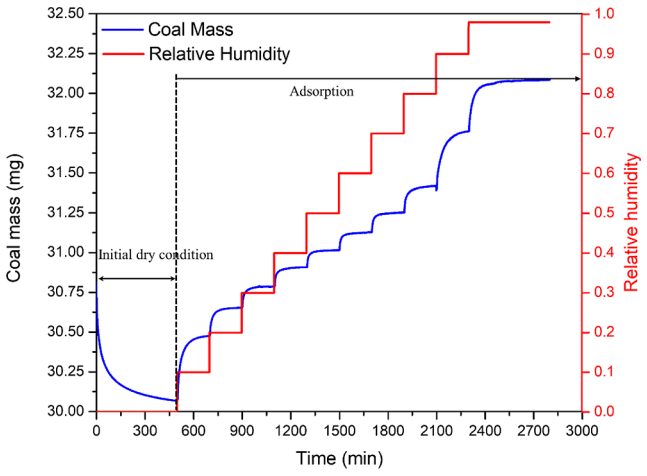

Figure 3. One full circle of water vapor adsorption measurement. Raw data recovered from the DVS analyzer for IS #6_Test 1.

residual water desorbs and the sample mass decreases as drying time evolves to a constant value taken as reference sample mass.[66] The equilibrium state under different relative humidities is defined when mass change is less than or equal to 0.002% per minute and maintained stable for at least 10 min. In Figure 3, the end value of the plateau at each relative humidity stage is regarded as M_∞ in eq 37.

4. RESULTS AND DISCUSSION

4.1. Sorption Isotherms of Moisture in Coal Samples. The sorption isotherms collected from IS #5_ Test 1, IS #5_ Test 2, and IS #5_ Test 3 for sample IS #5, and IS #6_ Test 1, IS #6_ Test 2, and IS #6_ Test 3 for sample IS #6 were fitted based on eq 3. Based on eq 3, the modeled results well agree with the experiment data ($R^2 > 0.99$), as summarized in Table 4. The three-time measurements confirm the data repeatability on water vapor sorption experiments. Based on the Langmuir-type sorption model, the maximum primary adsorption capacity represented by the parameter m_L corresponds to a complete monolayer coverage. By comparing the fitting results of the two sub-bituminous coal samples IS #5 and IS #6, the maximum primary adsorption capacity of IS #6 (averaged at

Table 4. Fitting Results in Figure 4 Based on eq 3

		fitting results			
sample		m_L	R_L	c	R^2
IS #5	test 1	0.0192	0.0349	0.885	0.995
	test 2	0.0200	0.0417	0.880	0.997
	test 3	0.0188	0.0369	0.886	0.996
	average	0.0193	0.038	0.884	0.996
IS #6	test 1	0.0224	0.0663	0.698	0.996
	test 2	0.0221	0.0631	0.714	0.996
	test 3	0.0221	0.0616	0.717	0.996
	average	0.0222	0.064	0.710	0.996

~0.0222 g/g) is slightly higher than IS #5 (~0.0193 g/g) (Table 4), which is in agreement with characterized surface oxidation degrees indicated by the O/C values in Table 3 and the more oxidized degree on coal sample IS #6 from Figure 1. The observations confirmed that the surface oxygen-containing group degree can determine the maximum water adsorption capacity during the primary adsorption stage mainly because the oxygen-containing functional groups on the coal surface offer hydrophilic sites with stronger primary water vapor uptake.[6,67,68]

4.2. Critical Relative Humidity for the Capillary Condensation. Based on the Kelvin equation, the critical relative humidity for specified pores can be theoretically derived. However, the pore size distribution of coal samples in Figure 2 combines nano- to macroscale pores. All these pores have the potential for capillary condensation. Capillary condensation may occur in nanoscale pores at low relative humidity, whereas capillary condensation may also occur in larger pores at higher relative humidity due to the formation of adsorbed water layers. It is quite challenging to theoretically define the exact value of critical relative humidity that distinguishes the multilayer adsorption stage and the capillary condensation stage. Based on the criteria defined in eq 23, capillary condensation start to occur in pores as the pore radius is less than the summation value of the radius of curvature of the interface $\mathcal{R}(h)$ and the thickness of the adsorbed layer ($t(h)$). Strictly, coal is a unique heterogeneity porous medium with dual porosity characteristics, which has very complex pore size distribution, as shown in Figure 2. To distinguish the multilayer adsorption stage from the capillary condensation stage, it is necessary to define the critical relative humidity with an exact value. For simplification, it should be noted that the critical relative humidityR_{hc} used represents a rough estimation value based on eq 26.

As quantified in eq 26, if there is no pore with small enough radius to allow capillary condensation, there exists a linear relation between the capillary pressure (i.e., $ln|P_c|$) and the volumetric water content (S_w). Based on eq 26, the results for both IS#5 and IS#6 are plotted in Figure 5a,b, respectively. The linear regressions for IS#5 and IS#6 were conducted several times. In Figure 5a,b, the well calibration results can be obtained between the selected range interval of relative humidity. The fitting goodness represented by the regression coefficients (R^2) are shown in both Figure 5a,b. The results show that the application of the linear relation for IS#5 can be well regressed over the relative humidity between 0.70 and 0.75 and the relative humidity between 0.70 and ~ 0.75 can be considered as the range interval that the critical relative humidity falls into. For IS#6, it shows that the linear regression was well regressed over the relative humidity between 0.70 and

https://doi.org/10.1021/acs.langmuir.2c02701
Langmuir 2022, 38, 14941−14958

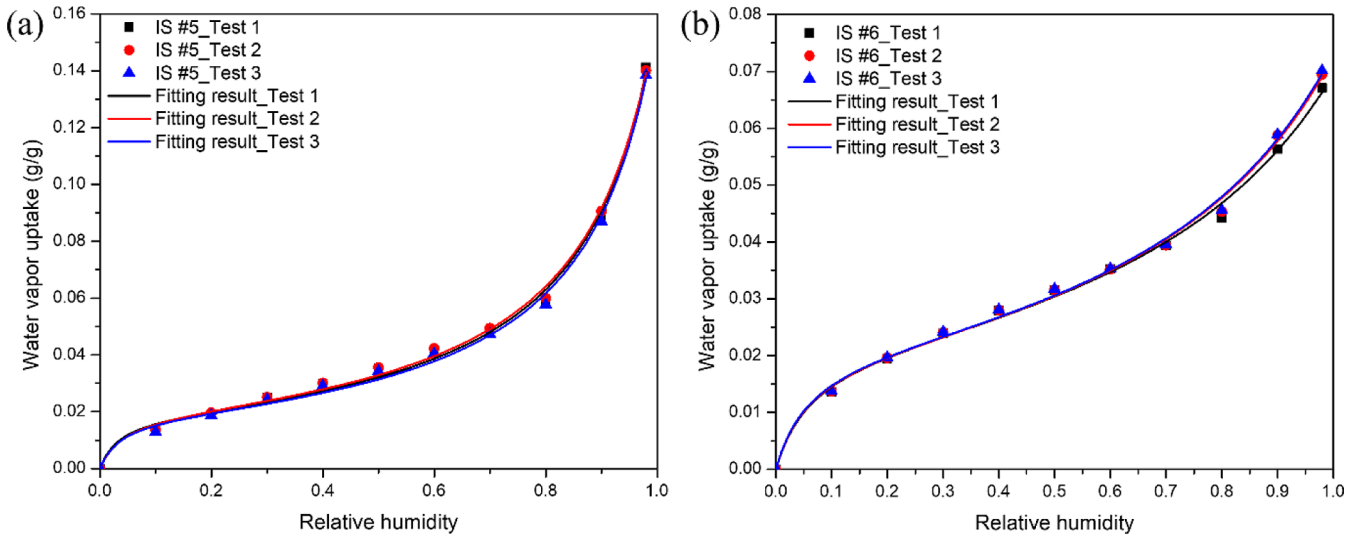

Figure 4. Comparisons between fitting results and experiment data. The water vapor sorption process can be generally divided into two stages including the primary adsorption and secondary adsorption.

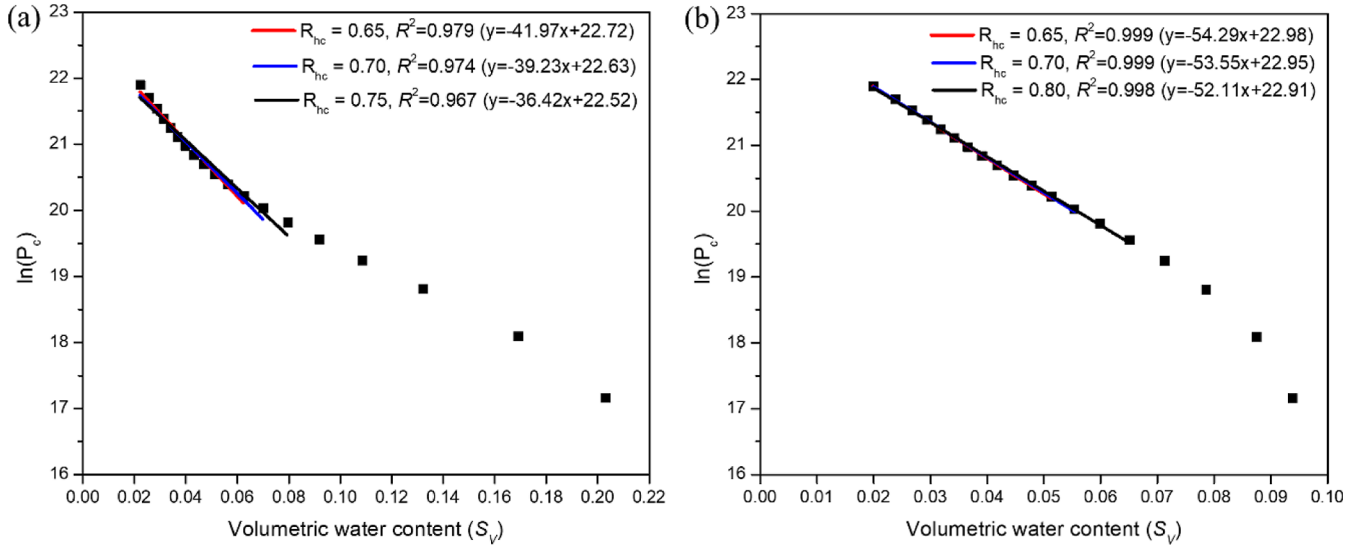

Figure 5. Critical relative humidity evaluation on two coal samples based on eq 26. (a) Sample IS#5. (b) Sample IS#6.

0.80. Similarly, the relative humidity between 0.70 and 0.80 for coal IS #6 can be regarded as the range interval that the critical relative humidity falls into.

4.3. Dynamic Diffusion Coefficients. Based on the theoretical analyses and experimental observations in Sections 2 and 3, the flow of water vapor in coal includes several flow regimes, namely, the combination flow of water molecules in vapor and adsorbed phases at low relative humidity range, flow of water molecules in the adsorbed phase with increasing relative humidity, and flow in capillary condensate at high relative humidity over the critical relative humidity point. Due to the different flow regimes, the apparent diffusion coefficients of water vapor flow in coal should be defined using stage-wise manner, as quantified in eq 35. The apparent diffusion coefficients of IS #5 and IS #6 as the relative humidity increases from 0.10 to 0.98 were estimated by using the unipore model, defined in eq 37. Because the coal particles for dynamic water vapor tests were prepared between 60 mesh to 80 mesh, it is hard to determine an equivalent particle size to calculate the diffusion coefficients from the effective diffusion coefficients. Thus, both the particle sizes at 60 mesh and 80 mesh were used to calculate the diffusion coefficients for restricting the upper and lower ranges. All the estimated diffusion coefficients are plotted in Figure 6, which are represented by points connected using shot-dash lines. To validate the proposed model in eq 35, the basic input parameters are summarized in Table 5. In Figure 6, the fitting results agree well with the experiment data. For both IS #5 and IS #6, the apparent diffusion coefficients shown non-linear relationships with respect to the relative humidity. It should be noted that the apparent diffusion coefficients of IS # 5 and IS #6 are piecewise functions of relative humidity. As an example, based on the results from Figure 5a, the relative humidity between 0.70 and 0.75 can be regarded as the range interval that the critical relative humidity falls into and thus the model validation results in Figure 6a can be divided into two parts based on eq 35.

Totally, at relatively low relative humidity stage, the apparent diffusion coefficients increase as the relative humidity increases, whereas they decrease with the relative humidity

https://doi.org/10.1021/acs.langmuir.2c02701
Langmuir 2022, 38, 14941−14958

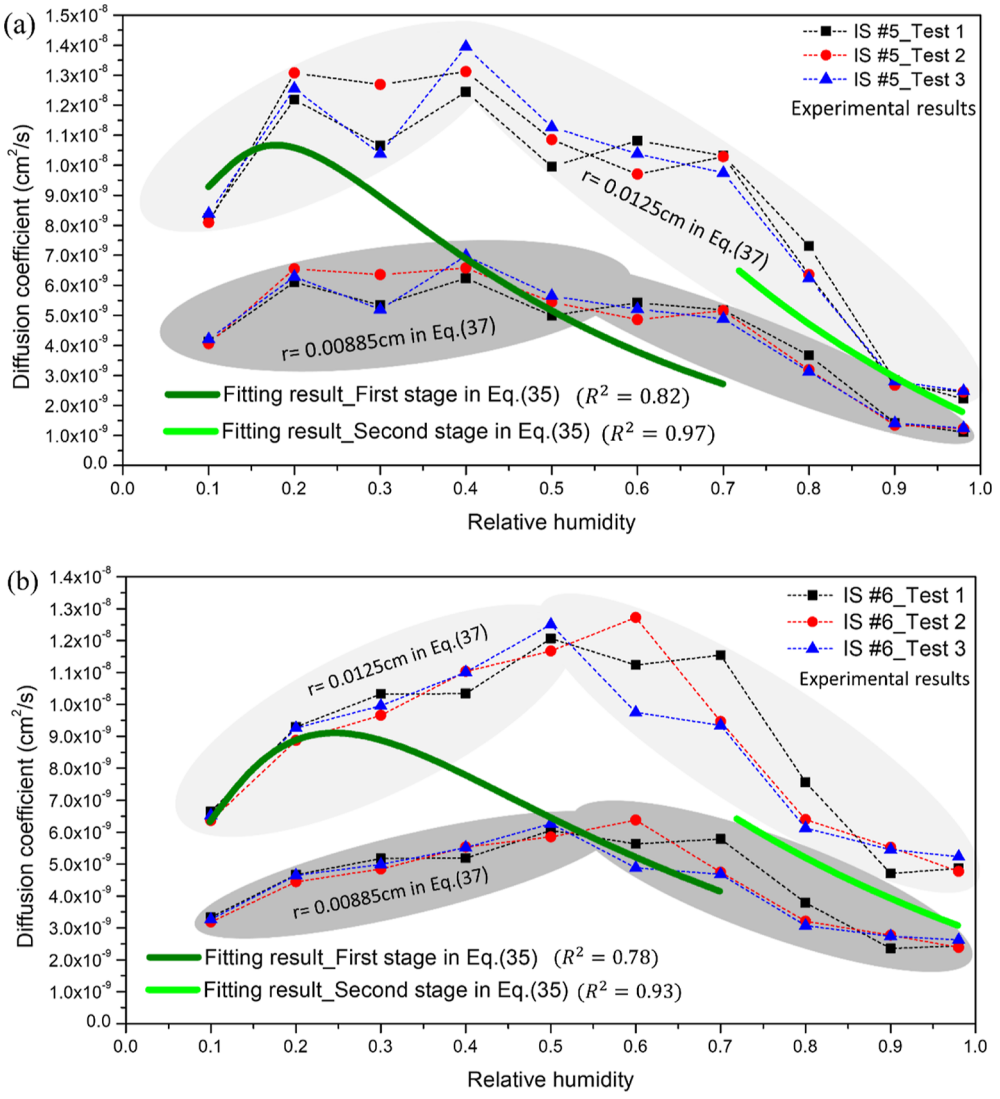

Figure 6. Comparisons between fitting results and experiment data on diffusion coefficients. (a) IS #5 and (b) IS #6. The experimental diffusion coefficients are represented by points connected using shot-dash lines. Upper and lower shaded areas represent the calculated diffusion coefficients using particle radii of 0.0125 cm and 0.00885 cm, respectively.

continuously increasing. For IS #5, the apparent diffusion coefficient increases from ~9.26 × 10^{-9} to 1.07 × 10^{-8} cm^2/s (~15.6%) as the relative humidity increases from ~0.10 to ~0.20, which subsequently decreases from 1.07 × 10^{-8} to 2.69 × 10^{-9} cm^2/s (~74.9%) as the relative humidity continuously increases up to a critical relative humidity of ~0.70. With the relative humidity continuously increasing up to ~0.98, the apparent diffusion coefficient finally decreases to 1.79 × 10^{-9} cm^2/s. For IS#6, the apparent diffusion coefficient increases from ~6.31 × 10^{-9} to 9.16 × 10^{-9} cm^2/s (~45.2%) as the relative humidity increases from ~0.10 to ~0.25, which subsequently decreases from 9.16 × 10^{-9} to 3.22 × 10^{-9} cm^2/s (~64.8%) as the relative humidity continuously increases up to a critical relative humidity of ~0.80. With the continuous increase in relative humidity up to ~0.98, the apparent diffusion coefficient finally decreases to 3.08 × 10^{-9} cm^2/s for IS #6. It should be noted that decreasing trends for both samples IS #5 and IS #6 before and after the critical humidity point show a little difference, which means that there has been a slight increase in diffusion coefficients near the critical point due to the contribution of flow in capillary condensate. The slight increase in diffusion coefficients influenced by capillary condensation is also confirmed by public data, as shown in Figure 7. The public data show that there exists a slight increase in the apparent diffusion coefficients as the capillary condensation occurs.

Based on the validated model, the contributions of different flow regimes at different stages to the total flow of moisture in coal samples are expected to be modeled and discussed. Under relatively lower relative humidity, namely, the flow of water molecules in the vapor phase and flow of water vapor in the adsorbed phase dominate during this period. For flow of water molecules in the vapor phase, as defined in eq 8, the term "$(1-S_w)$" represents the effective free pore space of the porous medium with continuous water vapor adsorption. This dynamic term continuously decreases with the increase of adsorbed water content. Upon reaching the equilibrium time, the effective pore volume will fully saturate with water and the mass flux induced by flow of water molecules in the vapor phase will cease. The contributions of flow in the free phase and the adsorbed phase can be evaluated through the weighting coefficients defined in eqs 31 and 32. As shown in

https://doi.org/10.1021/acs.langmuir.2c02701
Langmuir 2022, 38, 14941−14958

Table 5. Basic Input Parameters[a]

parameters	values	source
water vapor diffusion coefficient in free air, cm^2/s	0.242	NIST
water vapor compressibility factor, dimensionless	0.998	NIST
universal gas constant, J/(mol•K)	8.314	NIST
water molar mass, g/mol	18.0	NIST
saturated water vapor pressure at 303.15 K, kPa	4.24	NIST
water viscosity, Pa·s	7.97×10^{-4}	NIST
water vapor density, g/cm^3	3.0×10^{-5}	NIST
liquid water density, g/cm^3	1.0	NIST
surface tension coefficient of water, N/m	0.0712	NIST
Avogadro number, mol^{-1}	6.022×10^{23}	NIST
tortuosity	0.026 (IS #5);0.028 (IS #6)	modeling[69]
temperature, K	303.15	experimental test
coal density, g/cm^3	1.46 (IS #5);1.37 (IS #6)	experimental test
porosity	0.026 (IS #5);0.028 (IS #6)	experimental test
localized adsorption sites, mol/cm^3	0.00147 (IS #5) ;0.00180 (IS #6)	experimental test
coefficient of viscous flow resistance at stage I (α), $1/cm^2$	2.38×10^{16}(IS #5) ;3.52×10^{16}(IS #6)	regressed
coefficient of viscous flow resistance at stage II (α), $1/cm^2$	3.67×10^{17}(IS #5) ;7.24×10^{17}(IS #6)	regressed

[a]Coefficients of viscous flow resistance was fitted through the derived diffusion coefficient model and the measured diffusion coefficients. The water vapor diffusion constant in free air was obtained from NIST data, which was calibrated at a given temperature and thus the error bar was not included. The porosities of samples IS#5 and IS #6 were estimated based on LTNA tests. The viscosity of confined and interfacial water could be higher than the bulk phase. In addition, the viscosity of confined and interfacial water could also be dynamically changing with pore sizes and relative humidity. At this stage, we are confident in the derived formula while the input of the viscosity of confined water in pores is ideally assumed as the bulk phase.

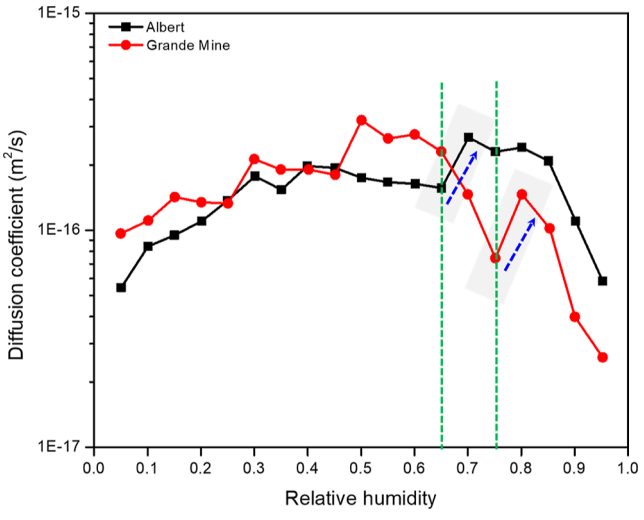

Figure 7. Diffusion coefficient of water vapor sorption in coal samples from public data.[17]

Figure 8, the flow of water molecules in the vapor phase contributes very less to the total mass flow, whereas the flow of water molecules in the adsorbed phase dominates the total mass flow in the first stage. For the flow of water molecules in the adsorbed phase, the spreading pressure continues to decrease with the increase in relative humidity based on eq 11. The decrease in spreading pressure can be converted to the decrease in flow velocity of the adsorbed phase. However, the increase in relative humidity will result in the increase in the amount of water molecules. By keeping in mind that the flow flux of water vapor in coal samples is the product of the flow velocity and the total adsorbed amount of water molecules, the apparent mass transfer induced by flow in the adsorbed phase should have a critical point. Here, the critical point means the relative humidity that before which the increase in the amount of adsorbed water molecules dominate the total mass flow (i.e., monolayer adsorption stage or early multilayer adsorption stage), then after which the mass flow velocity decreases dramatically and thus very slow mass transfer. With relative humidity continuously increasing, flow in capillary condensate occurs, which will dominate the total mass flow. The results show that the early stage of capillary condensation will induce a slightly higher diffusion coefficient. However, the apparent diffusion coefficients continuously decrease as the relative humidity increases, as illustrated in Figure 6.

To summarize, the apparent diffusion coefficient of moisture in coal samples with respect to relative humidity can be divided into three stages, as illustrated in Figure 9. In the first stage, before the relative humidity of R_{hc1}, the fast diffusion induced by flow of water molecules in the vapor phase and the relatively slow diffusion of surface flow induced by monolayer or multilayer adsorption constitute the total mass transfer, whereas the apparent diffusion at this stage is still dominated by surface flow of water molecules in the adsorbed phase due to the very less mass weight of water vapor indexed by the weighting coefficients as shown in Figure 9. At the second stage, with the relative humidity rangings from R_{hc1} to R_{hc2}, the contribution of free water vapor flow to the apparent flow is restricted mainly due to the narrow effect of the effective pore space, as quantified by the term "$(\phi - S_w)$" in eq 11. Thus, the mass flux contribution induced by water vapor flow in the free phase can be neglected during the second stage and the surface flow of water molecules in the adsorbed phase dominates. In Figure 9, the diffusion coefficient D_a indicates that the capacity of surface flow in the adsorbed phase is modeled from eq 18. With relative humidity continuously increasing, upon reaching the critical relative humidity, the capillary condensation will dominate the total mass flow and the mass transfer process of water molecules in coal samples during the third stage. At the early time of this stage, there will be a slight increase in diffusion speed than the end time of the last stage but which will continuously decrease as the relative humidity increases. It should be noted that Figure 9 gives the full contributions of different diffusion regimes based on eq 35. However, the application of eq 35 is highly related to the water adsorption behavior.

5. DISCUSSION

5.1. Matrix Swelling/Shrinkage of Colloidal Gel-like Coal in Response to Moisture Gain/Loss. It is well established that coal has a colloidal gel structure that can shrink and swell in response to moisture loss and gain,[54,70] which can be explained based on the "Bingham effect" theory (adsorption-induced expansion in the thin-film adsorption regime).[71] The properties of swellable coal implied that the belief that coal holds a significant portion of its moisture via

https://doi.org/10.1021/acs.langmuir.2c02701
Langmuir 2022, 38, 14941−14958

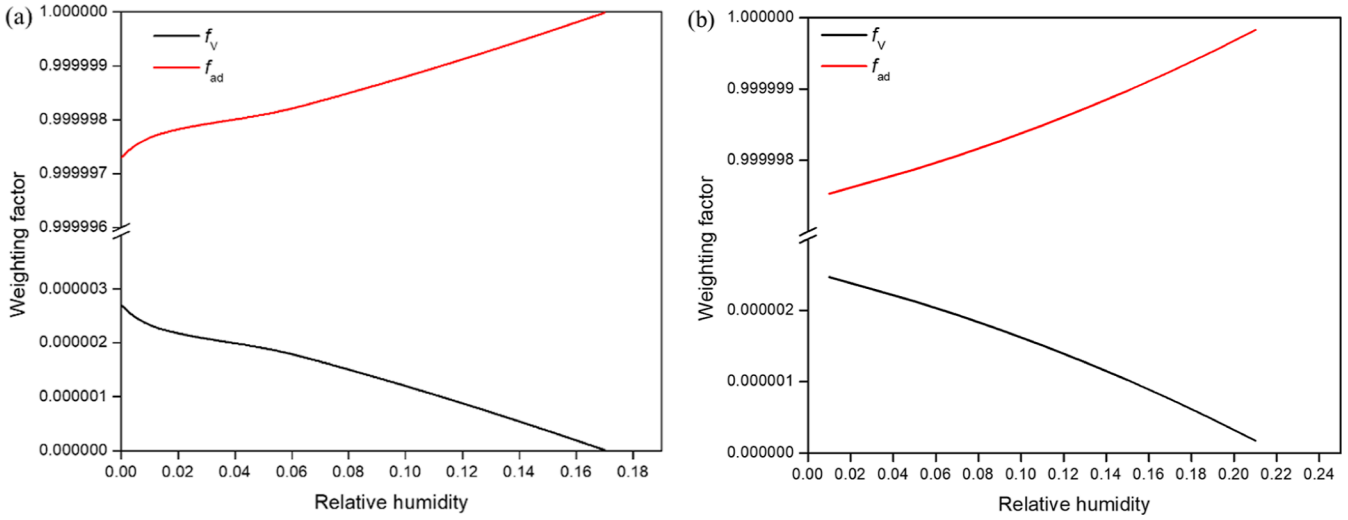

Figure 8. Variations of weighting factors with respect to relative humidity. (a) IS#5. (b) IS#6.

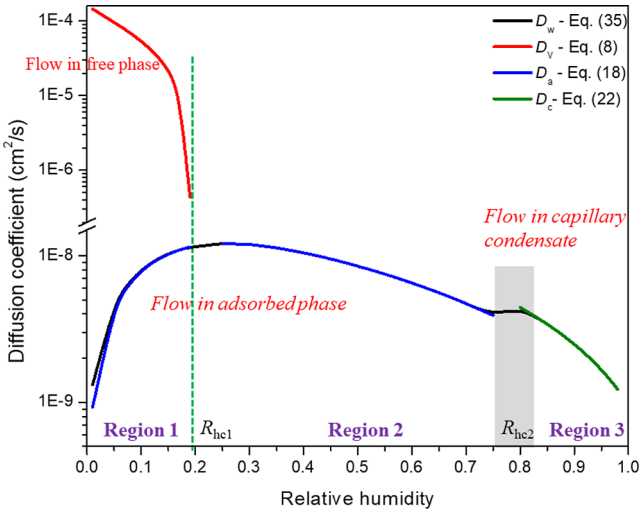

Figure 9. Apparent diffusion coefficient of moisture sorption in coal samples at a given relative humidity.

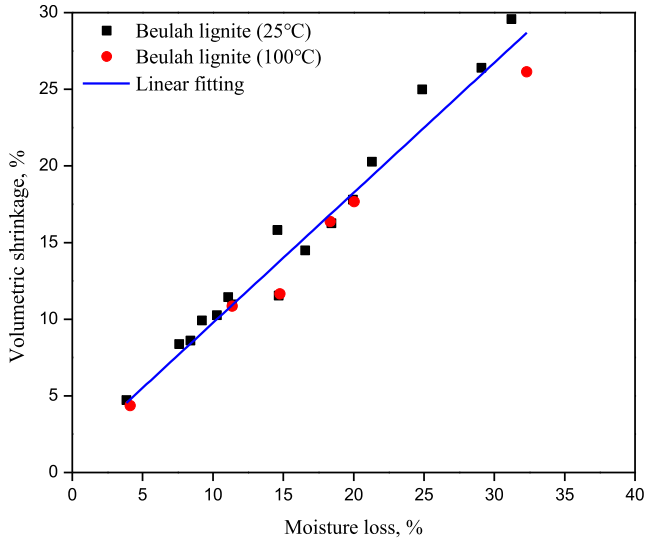

Figure 10. Volumetric shrinkage of lignite upon drying at two different temperatures.[70]

capillary condensation processes is possibly in error.[70] In addition, the collapse of coal structure under varying relative humidity can influence the transport behaviors of fluids in coals.[70] Suuberg et al. studied the role of moisture in coal structure and the effects of drying on the accessibility of coal structure. It was observed that the more severe the drying of lignite, the more its porosity would collapse, and the apparent surface area would be much more lower.[70] As plotted in Figure 10, the volumetric shrinkage of coals with decreasing relative humidity is correlated by volumetric shrinkage (%) = 0.863 (moisture content, weight %)—0.162. In addition, the experimental results showed that the volumetric shrinkage appears to correlate linearly with the mass loss of moisture from the coals for coals ranging from lignite to bituminous in rank.[70]

Figure 10 shows the volumetric shrinkage of coal upon drying through controlling temperature. Deevi and Suuberg also measured the macroscopic shrinkages on larger cubic lignite samples from North Dakota through decreasing relative humidity.[72] Under the assumption that all pores in coals are initially filled with water and any water removed has a specific volume of 1 cm^3/g, the measured macroscopic shrinkages and the volumetric shrinkages were compared, as shown in Figure 11. For all the samples, pore collapses occur to some extents at certain relative humidities that were much greater than predicted on the basis of simple bulk water removing.[72] Suuberg et al. also conducted other studies based on solvent swelling examinations of coals through soaking with water that reached similar conclusions.[73] Thus, it should be noted that the colloidal gel structure has significant influences on mechanism-based understandings of water vapor transport behavior in nanoporous coal, which will be further studied in the future.

5.2. Coal Structure Collapse as Consequences of Matric Suction Evolution. The volumetric shrinkage results as shown in both Figures 10 and 11 confirmed that the coal structure collapses upon drying. The further question is to which dimension scale is the pore structure to occur collapse upon drying. The swelling data of coal samples upon drying as shown in Table 6 is adopted from Deevi and Suuberg. The data imply that there exists the irreversible pore collapse at relatively high values of R_h and most of the pore collapses are observed on drying to a relative humidity of 0.75. By recalling

https://doi.org/10.1021/acs.langmuir.2c02701
Langmuir 2022, 38, 14941−14958

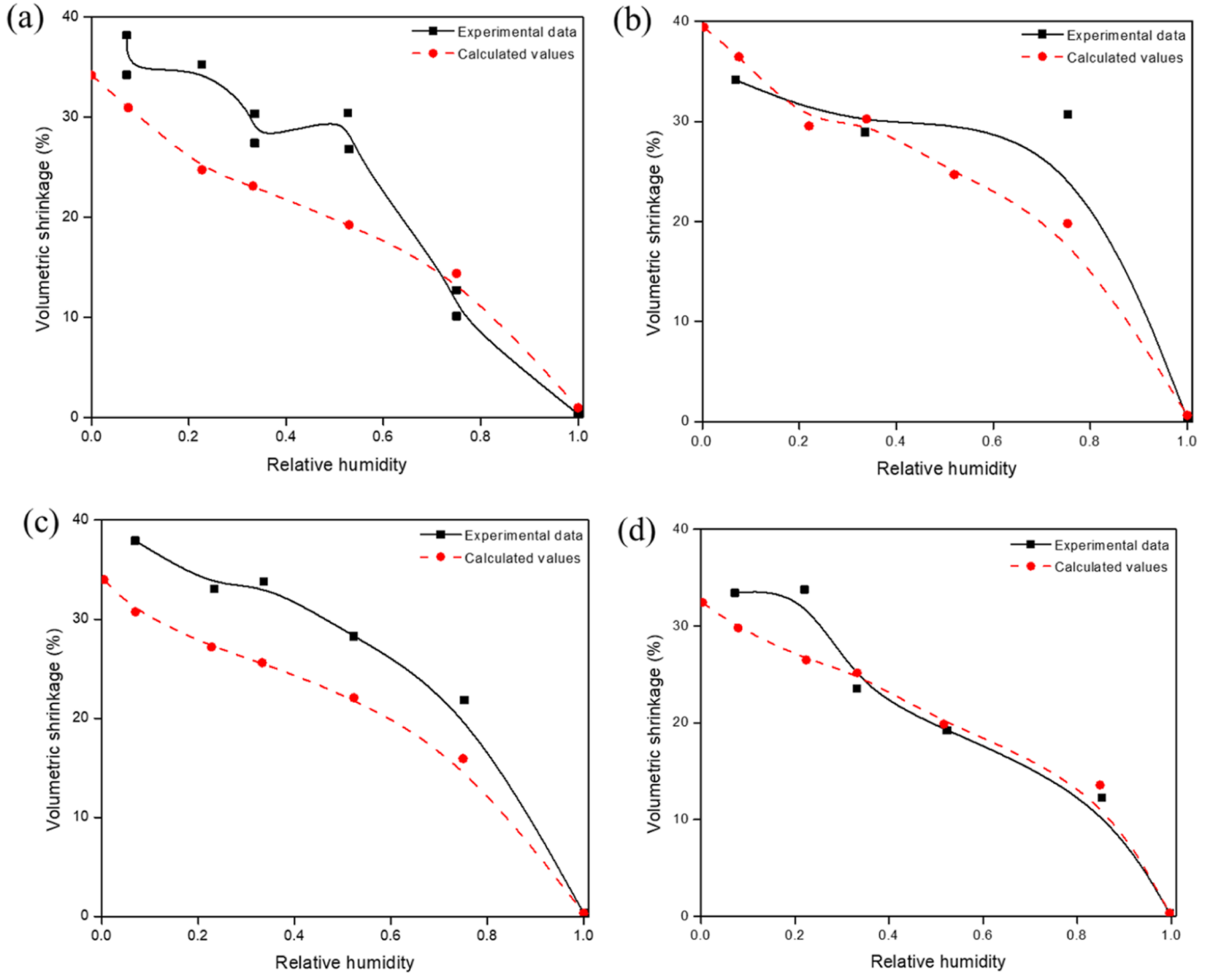

Figure 11. Volumetric shrinkage of lignites with respect to the relative humidity.[72] (a) Freedom sample. (b) Gascoyne sample. (c) Glenn Harold sample. (d) Beulah sample.

Table 6. Swelling of Dried Samples[72]

samples	R_h for drying	forms*	swelling ratio (Vfinal/Vdry)	recovery (%)
Glenn Harold	0.75	cube	1.09	85
	0.75	powder	1.12	87
	0.33	cube	1.29	85
	0.33	powder	1.18	78
	0.00	powder	1.35	
Gascoyne	0.75	cube	1.11	78
	0.75	powder	1.10	77
	0.00	powder	1.42	
Freedom	0.33	cube	1.19	83
	0.33	powder	1.19	83
	0.22	cube	1.25	81
	0.22	powder	1.22	79
	0.00	powder	1.27	
Beulah	0.00	powder	1.19	

the Kelvin equation in eq 38, the pore size is expected to be estimated as[72]

$$\ln(R_h) = -\frac{2\gamma V_m \cos\theta}{r_p RT} \tag{38}$$

where V_m is the water molar volume, cm^3/mol and θ is the contact angle.

Under the assumption of perfect wetting of the pore walls by water, the contact angle θ is assumed as zero, γ is 71.18 mN/m, V_m is 18.09 cm^3/mol, R is 8.314 J/(mol·K), T is 303.15 K, and the pores of ~7 nm were involved at R_h of 0.75. Because of the interfacial tension at the air−water interface, the vapor pressure u_a is larger than that in the liquid phase u_w and the capillary suction is thus initiated. The capillary suction can be given based on the Young−Laplace equation, expressed as[74]

$$u_a - u_w = \frac{2\gamma \cos\theta}{r_p} \tag{39}$$

where $u_w - u_a$ is the suction potential, which is the pressure difference between pore-water and pore-air, kPa; u_w is the pore-water pressure, kPa; and u_a is the pore-air pressure, kPa.

Based on eqs 38 and 39, the matric suction with respect to the relative humidity can be established as

https://doi.org/10.1021/acs.langmuir.2c02701
Langmuir 2022, 38, 14941−14958

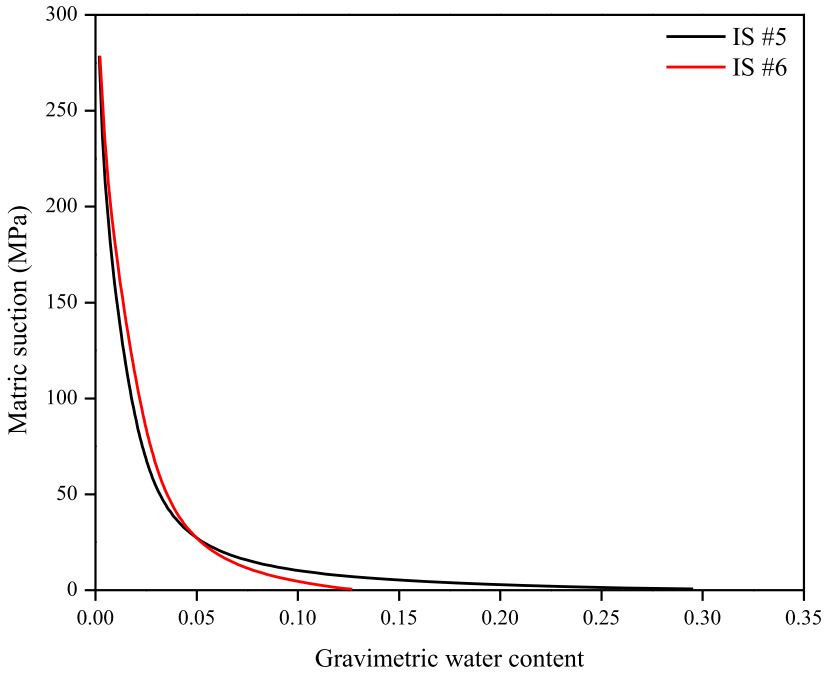

Figure 12. Matric suction variations with respect to moisture in samples IS #5 and IS #6.

$$u_a - u_w = -\frac{RT}{V_m}\ln(R_h) \tag{40}$$

According to eq 40, the matric suctions in both coal samples IS#5 and IS#6 are estimated, as shown in Figure 12. The results show that the matric suction significantly increases as the relative humidity decreases.

Matric suction generating on the interface of liquid water and solid wall surface has been recognized as the reason for the stability in non-cohesive soils. The improved effective stress evolution within the unsaturated porous medium can be expressed as[75]

$$\sigma_e = \sigma_t - u_a + \chi(u_a - u_w) \tag{41}$$

where σ_e is effective stress for unsaturated, MPa; σ_t is the total stress, MPa; and χ is the coefficient related to the water saturation degree, which is unity for a saturated soil and zero for a dry soil. Based on eq 41, it appears that the effective stress acting on the coal matrix will increase with the increase in matric suction, where the local coal failure may potentially occur based on the Mohr−Coulomb shear or maximum tensile stress failure criteria. It seems that the pore collapse phenomenon under such high effective stress is reasonable, but which need further experimental evidences both in macro- and micro-scale.

6. CONCLUSIONS

This study provides a systematic method to characterize the moisture retention and multi-mechanistic transport behaviors in nanoporous coal. Based on this study, the following conclusions can be made:

(1) A mechanism-based isotherm model was proposed to estimate the water vapor uptake at various relative humidities. The integrated isotherm model implicitly coupled the monolayer adsorption, multilayer adsorption, and capillary condensation, which is constrained by the dynamic water vapor sorption data.

(2) As the relative humidity increases from ∼0.10 to ∼0.98, the apparent diffusion coefficients for IS #5 increases from ∼9.26×10^{-9} to 1.07×10^{-8} cm^2/s and finally decreases to 1.79×10^{-9} cm^2/s. For IS#6, the apparent diffusion coefficient increases from ∼6.31×10^{-9} to 9.16×10^{-9} cm^2/s and finally decreases to 3.08×10^{-9} cm^2/s.

(3) The contributions of different diffusion regimes to the total mass flow were discussed. At the first stage, the fast diffusion induced by flow of water molecules in the vapor phase and the relatively slow diffusion of surface flow induced by monolayer or multilayer adsorption constitute the total mass transfer whereas the apparent diffusion at this stage is still dominated by surface flow of water molecules in the adsorbed phase due to the very less mass weight of water vapor indexed by the weighting coefficients; during the second stage, the contribution of free water vapor flow to the apparent flow can be neglected and the mass transfer at this stage is still dominated by the surface flow; upon reaching the critical relative humidity, the flow in capillary condensation will dominate the total mass flow.

(4) Coal structure collapse upon drying may be induced by high matric suction with associated low water content, which is intensively related to coal ranks and has significant influences on mechanism-based understandings of moisture transport behavior in nanoporous coals.

AUTHOR INFORMATION

Corresponding Author

Shimin Liu − *Department of Energy and Mineral Engineering, G³ Center and Energy Institute, The Pennsylvania State University, University Park, Pennsylvania 16802, United States;* orcid.org/0000-0001-9612-0047; Email: szl3@psu.edu

https://doi.org/10.1021/acs.langmuir.2c02701
Langmuir 2022, 38, 14941−14958

Authors

Ang Liu − *Department of Energy and Mineral Engineering, G³ Center and Energy Institute, The Pennsylvania State University, University Park, Pennsylvania 16802, United States*

Kai Wang − *School of Emergency Management and Safety Engineering, China University of Mining and Technology (Beijing), Beijing 100083, China*

Complete contact information is available at: https://pubs.acs.org/10.1021/acs.langmuir.2c02701

Notes

The authors declare no competing financial interest.

■ ACKNOWLEDGMENTS

This work was financially supported by The National Institute for Occupational Safety and Health (NIOSH) under contract no. NIOSH-75D30119C05128.

■ NOMENCLATURE

R_h	relative humidity, dimensionless
m_{pri}	primary adsorption capacity, g/g
m_{sec}	secondary adsorption capacity, g/g
m	total adsorption capacity, g/g
m_L	maximum primary adsorption capacity, g/g
R_L	primary adsorption constant, dimensionless
p_V	partial pressure of water vapor at a specified temperature T, kPa
p_{VS}	saturated pressure of water vapor at a specified temperature T, kPa
T	temperature, K
m_0	prioritized adsorption capacity for secondary adsorption, g/g
c	secondary adsorption constant, dimensionless
k	loss of the secondary sites during secondary adsorption, dimensionless
ω	ratio of primary adsorption sites provided for secondary adsorption, dimensionless
q_V	vapor flux of water molecules in the vapor phase, mol/(cm²•s)
D_0	diffusion coefficient of free water vapor in air, cm²/s
M	molar mass of water, g/mol
ϕ	porosity, dimensionless
τ	tortuosity, dimensionless
ρ_V	mass density of water vapor in the free phase, g/cm³
ρ_{VS}	mass density of saturated water vapor under a given temperature, g/cm³
u_a	flow velocity of water molecules in the adsorbed phase, cm/s
q_a	surface flow flux of water molecules in the vapor phase, mol/(cm²•s)
C_a	water molecular concentration in the adsorbed phase, mol/cm³
m_t	total mass of adsorbed water molecules, g
V_c	coal volume, cm³
V_w	total volume of adsorbed water molecules, cm³
p_c	capillary pressure, Pa
$\mathcal{R}(h)$	radius of curvature of a capillary interface, nm
u_c	flow velocity of water molecules in the capillary condensate phase, cm/s
r_p	pore radius, nm
$\eta(r_p)$	volume fraction of pores with radii smaller than r_p, dimensionless
a	regression parameter
b	regression parameter
m_f	content of water molecules in the vapor phase, g/cm³
q_t	total flux of water molecules at the first stage, mol/(cm²•s)
C_t	total water molecular concentration at the first stage, mol/cm³
D_{af}	apparent diffusion coefficient at the first stage, cm²/s
r	particle radius, cm
M_t	masses of water molecules adsorbed at time t, g
V_m	water molar volume, cm³/mol
u_a	pore air pressure, kPa
σ_e	effective stress, MPa
σ_t	total stress, MPa
A	surface area per unit volume, cm²/cm³
S_V	volumetric water content, cm³/cm³
ρ_c	mass density of coal, g/cm³
ρ_{lw}	mass density of liquid water, g/cm³
q	flow flux induced by diffusion defined in Fick's law, mol/(cm²•s)
D	diffusion coefficient defined in Fick's law, cm²/s
C	fluid concentration defined in Fick's law adsorbed gas concentration, mol/cm³
C_V	water molecular concentration in the free phase, mol/cm³
V_p	pore volume, cm³
R	universal gas constant, J/(mol·K)
Z	compressibility factor of water vapor, dimensionless
D_V	diffusion coefficient of water vapor in the vapor phase, cm²/s
ρ	fluid density, g/cm³
u	fluid velocity, cm/s
P	fluid pressure, N/cm
F	external force of a volume element, g/(cm²•s²)
ψ	viscous resisting force acting on a unit volume, g/(cm²•s²)
α	coefficient of viscous flow resistance, 1/cm²
μ	water viscosity, Pa•s
p_s	spreading pressure, Pa
n	maximum number concentration of primary adsorption sites, mol/cm³
n_s	actual number concentration of water molecules adsorbed on primary adsorption sites, mol/cm³
n_t	total number concentration of water molecules adsorbed on both primary and secondary adsorption sites, mol/cm³
N_t	total number of water molecules adsorbed on both primary and secondary adsorption sites, mol
m_c	coal mass, g
D_a	diffusion coefficient of water molecules in the adsorbed phase, cm²/s
n_V	molar amount of water vapor molecules in the free phase, mol
γ	surface tension coefficient, N/cm
q_c	flow flux of water molecules in the capillary condensate phase, mol/(cm²•s)
D_c	diffusion coefficient of water molecules in the capillary condensate phase, cm²/s
$t(h)$	thickness of the adsorbed layer, nm
$S(r_p)$	area of pores of radii larger than r_p, cm²/cm³

$S(0)$ total area of pores per unit volume, cm^2/cm^3
R_{hc} critical relative humidity, dimensionless
m_{ad} content of water molecules in the adsorbed phase, g/cm^3
f_V weighting factor for flow flux in the free vapor phase, dimensionless
f_{ad} weighting factor for flow flux in the adsorbed phase, dimensionless
D_w general form apparent diffusion coefficient, cm^2/s
t time, s
M_∞ masses of water molecules adsorbed at equilibrium time t, g
θ contact angle, degree
u_w pore water pressure, kPa
χ coefficient related to water saturation degree, dimensionless
S_w water saturation, dimensionless

REFERENCES

(1) Chen, D.; Pan, Z.; Liu, J.; Connell, L. D. Modeling and Simulation of Moisture Effect on Gas Storage and Transport in Coal Seams. *Energy Fuel.* **2012**, *26*, 1695−1706.
(2) Chen, D.; Pan, Z.; Liu, J.; Connell, L. D. An Improved Relative Permeability Model for Coal Reservoirs. *Int. J. Coal Geol.* **2013**, *109*−*110*, 45−57.
(3) Liu, A.; Wang, K.; Zang, J.; Du, F.; Zhou, A. Relative Permeability of Gas for Unconventional Reservoirs. *Transp. Porous Media* **2018**, *124*, 289−307.
(4) Wang, S.; Elsworth, D.; Liu, J. Permeability evolution in fractured coal: The roles of fracture geometry and water-content. *Int. J. Coal Geol.* **2011**, *87*, 13−25.
(5) Wang, K.; Zang, J.; Feng, Y.; Wu, Y. Effects of Moisture on Diffusion Kinetics in Chinese Coals during Methane Desorption. *J. Nat. Gas Sci. Eng.* **2014**, *21*, 1005−1014.
(6) Busch, A.; Gensterblum, Y. CBM and CO2-ECBM related sorption processes in coal: A review. *Int. J. Coal Geol.* **2011**, *87*, 49−71.
(7) Ahamed, M. A. A.; Perera, M. S. A.; Matthai, S. K.; Ranjith, P. G.; Dong-yin, D. Coal composition and structural variation with rank and its influence on the coal-moisture interactions under coal seam temperature conditions - A review article. *J. Pet. Sci. Eng.* **2019**, *180*, 901−917.
(8) Pan, Z.; Connell, L. D.; Camilleri, M.; Connelly, L. Effects of Matrix Moisture on Gas Diffusion and Flow in Coal. *Fuel* **2010**, *89*, 3207−3217.
(9) Liu, A.; Liu, S. Mechanical property alterations across coal matrix due to water-CO2 treatments: A micro-to-nano scale experimental study. *Energy* **2022**, *248*, 123575.
(10) Liu, A.; Liu, S. A fully-coupled water-vapor flow and rock deformation/damage model for shale and coal: Its application for mine stability evaluation. *Int. J. Rock Mech. Min. Sci.* **2021**, *146*, 104880.
(11) Pan, Z. Modeling of Coal Swelling Induced by Water Vapor Adsorption. *Front. Chem. Sci. Eng.* **2012**, *6*, 94−103.
(12) Ozdemir, E.; Schroeder, K. Effect of Moisture on Adsorption Isotherms and Adsorption Capacities of CO2on Coals. *Energy Fuel.* **2009**, *23*, 2821−2831.
(13) Liu, J.; Peach, C. J.; Spiers, C. J. Anisotropic swelling behaviour of coal matrix cubes exposed to water vapour: Effects of relative humidity and sample size. *Int. J. Coal Geol.* **2016**, *167*, 119−135.
(14) Day, S.; Sakurovs, R.; Weir, S. Supercritical Gas Sorption on Moist Coals. *Int. J. Coal Geol.* **2008**, *74*, 203−214.
(15) Goodman, A. L.; Busch, A.; Bustin, R. M.; Chikatamarla, L.; Day, S.; Duffy, G. J.; Fitzgerald, J. E.; Gasem, K. A. M.; Gensterblum, Y.; Hartman, C.; Jing, C.; Krooss, B. M.; Mohammed, S.; Pratt, T.; Robinson, R. L.; Romanov, V.; Sakurovs, R.; Schroeder, K.; White, C. M. Inter-laboratory comparison II: CO2 isotherms measured on moisture-equilibrated Argonne premium coals at 55 °C and up to 15 MPa. *Int. J. Coal Geol.* **2007**, *72*, 153−164.
(16) Allardice, D. J.; Evans, D. G. The-Brown Coal/Water System: Part 2. Water Sorption Isotherms on Bed-Moist Yallourn Brown Coal. *Fuel* **1971**, *50*, 236−253.
(17) Charrière, D.; Behra, P. Water Sorption on Coals. *J. Colloid Interface Sci.* **2010**, *344*, 460−467.
(18) Furmaniak, S.; Gauden, P. A.; Terzyk, A. P.; Rychlicki, G. Water Adsorption on Carbons - Critical Review of the Most Popular Analytical Approaches. *Adv. Colloid Interface Sci.* **2008**, *137*, 82−143.
(19) Kaji, R.; Muranaka, Y.; Otsuka, K.; Hishinuma, Y. Water Absorption by Coals: Effects of Pore Structure and Surface Oxygen. *Fuel* **1986**, *65*, 288−291.
(20) McCutcheon, A. L.; Barton, W. A.; Wilson, M. A. Characterization of Water Adsorbed on Bituminous Coals. *Energy Fuel.* **2003**, *17*, 107−112.
(21) Švábová, M.; Weishauptová, Z.; Přibyl, O. Water Vapour Adsorption on Coal. *Fuel* **2011**, *90*, 1892−1899.
(22) Liu, L.; Tan, S.; Horikawa, T.; Do, D. D.; Nicholson, D.; Liu, J. Water Adsorption on Carbon - A Review. *Adv. Colloid Interface Sci.* **2017**, *250*, 64−78.
(23) Do, D. D.; Junpirom, S.; Do, H. D. A New Adsorption-Desorption Model for Water Adsorption in Activated Carbon. *Carbon* **2009**, *47*, 1466−1473.
(24) Wan, K.; He, Q.; Miao, Z.; Liu, X.; Huang, S. Water Desorption Isotherms and Net Isosteric Heat of Desorption on Lignite. *Fuel* **2016**, *171*, 101−107.
(25) Thommes, M.; Kaneko, K.; Neimark, A. V.; Olivier, J. P.; Rodriguez-Reinoso, F.; Rouquerol, J.; Sing, S. W. Physisorption of Gases, with Special Reference to the Evaluation of Surface Area and Pore Size Distribution (IUPAC Technical Report). *Pure Appl. Chem.* **2015**, *87*, 1051−1069.
(26) Brunauer, S.; Emmett, P. H.; Teller, E. Adsorption of Gases in Multimolecular Layers. *J. Am. Chem. Soc.* **1938**, *60*, 309−319.
(27) Anderson, R. B. Modifications of the Brunauer, Emmett and Teller Equation1. *J. Am. Chem. Soc.* **1946**, *68*, 686−691.
(28) Langmuir, I. The Constitution and Fundamental Properties of Solids and Liquids. Part I. Solids. *J. Am. Chem. Soc.* **1916**, *38*, 2221−2295.
(29) Guggenheim, E. A.*Applications of Statistical Mechanics*; Clarendon Press: Oxford, 1966.
(30) Dubinin, M. M. Water Vapor Adsorption and the Microporous Structures of Carbonaceous Adsorbents. *Carbon* **1980**, *18*, 355−364.
(31) deBoer, J. H.*The Dynamical Character of Adsorption*; Clarendon Press: Oxford, 1953.
(32) D'Arcy, R. L.; Watt, I. C. Analysis of Sorption Isotherms of Non-Homogeneous Sorbents. *Trans. Faraday Soc.* **1970**, *66*, 1236−1245.
(33) Malakhov, A. O.; Volkov, V. V. Cooperative Multimolecular Sorption Equation: Application to an Alcohol−Poly(1-trimethylsiyl-1-propyne) System. *Polym. Sci., Ser. A* **2000**, *42*, 1728−1729.
(34) Do, D. D.; Do, H. D. A Model for Water Adsorption in Activated Carbon. *Carbon* **2000**, *38*, 767−773.
(35) Harpalani, S.; Chen, G. Estimation of Changes in Fracture Porosity of Coal with Gas Emission. *Fuel* **1995**, *74*, 1491−1498.
(36) Palmer, I.; Mansoori, J. How Permeability Depends on Stress and Pore Pressure in Coalbeds: A New Model. *SPE Reservoir Eval. Eng.* **1998**, *1*, 539−544.
(37) Pan, Z.; Connell, L. D. Modelling of Anisotropic Coal Swelling and Its Impact on Permeability Behaviour for Primary and Enhanced Coalbed Methane Recovery. *Int. J. Coal Geol.* **2011**, *85*, 257−267.
(38) Liu, S.; Harpalani, S.; Pillalamarry, M. Laboratory Measurement and Modeling of Coal Permeability with Continued Methane Production: Part 2 - Modeling Results. *Fuel* **2012**, *94*, 117−124.
(39) Moore, R.; Palmer, I.; Higgs, H. Anisotropic Model for Permeability Change in Coalbed-Methane Wells. *SPE Reservoir Eval. Eng.* **2015**, *18*, 456−462.
(40) Saurabh, S.; Harpalani, S. Anisotropy of Coal at Various Scales and Its Variation with Sorption. *Int. J. Coal Geol.* **2019**, *201*, 14−25.

https://doi.org/10.1021/acs.langmuir.2c02701
Langmuir 2022, 38, 14941−14958

(41) Krishna, R.; Wesselingh, J. A. The Maxwell-Stefan Approach to Mass Transfer. *Chem. Eng. Sci.* **1997**, *52*, 861−911.
(42) Wang, Y.; Liu, S.; Zhao, Y. Modeling of Permeability for Ultra-Tight Coal and Shale Matrix: A Multi-Mechanistic Flow Approach. *Fuel* **2018**, *232*, 60−70.
(43) Abeles, B.; Chen, L. F.; Johnson, J. W.; Drake, J. M. Capillary Condensation and Surface Flow in Microporous Vycor Glass. *Isr. J. Chem.* **1991**, *31*, 99.
(44) Gruener, S.; Hofmann, T.; Wallacher, D.; Kityk, A. V.; Huber, P. Capillary Rise of Water in Hydrophilic Nanopores. *Phys. Rev. E* **2009**, *79*, 067301.
(45) Jani, A.; Busch, M.; Mietner, J. B.; Ollivier, J.; Appel, M.; Frick, B.; Zanotti, J. M.; Ghoufi, A.; Huber, P.; Fröba, M.; Morineau, D. Dynamics of Water Confined in Mesopores with Variable Surface Interaction. *J. Chem. Phys.* **2021**, *154*, 094505.
(46) Sang, G.; Liu, S.; Elsworth, D.; Zhang, R.; Bleuel, M. Pore-Scale Water Vapor Condensation Behaviors in Shales: An Experimental Study. *Transp. Porous Media* **2020**, *135*, 713−734.
(47) Ortiz-Young, D.; Chiu, H. C.; Kim, S.; Voïtchovsky, K.; Riedo, E. The Interplay between Apparent Viscosity and Wettability in Nanoconfined Water. *Nat. Commun.* **2013**, *4*, 2482.
(48) Dubinin, M. M.; Zaverina, E. D.; Serpinsky, V. V. The Sorption of Water Vapour by Active Carbon. *J. Chem. Soc.* **1955**, 1760−1766.
(49) Barton, S. S.; Evans, M. J. B.; MacDonald, J. A. F. Adsorption of Water Vapor on Nonporous Carbon. *Langmuir* **1994**, *10*, 4250−4252.
(50) Freeman, G. B.; Reucroft, P. J. Adsorption of HCN and H2O vapor mixtures by activated and impregnated carbons. *Carbon* **1979**, *17*, 313−316.
(51) Tarasevich, Y. I.; Aksenenko, E. V. Interaction of Water, Methanol and Benzene Molecules with Hydrophilic Centres at a Partially Oxidised Model Graphite Surface. *Colloids Surf., A* **2003**, *215*, 285−291.
(52) Philip, J. R.; De Vries, D. A. Moisture Movement in Porous Materials under Temperature Gradients. *Trans., Am. Geophys. Union* **1957**, *38*, 222−232.
(53) Fick, A. On Liquid Diffusion. *J. Membr. Sci.* **1995**, *100*, 33−38.
(54) Choi, J. G.; Do, D. D.; Do, H. D. Surface Diffusion of Adsorbed Molecules in Porous Media: Monolayer, Multilayer, and Capillary Condensation Regimes. *Ind. Eng. Chem. Res.* **2001**, *40*, 4005−4031.
(55) Babbitt, J. D. On the Differential Equations of Diffusion. *Can. J. Res.* **1950**, *28*, 449−474.
(56) Geertsma, J. Estimating the Coefficient of Inertial Resistance in Fluid Flow Through Porous Media. *SPE J.* **1974**, *14*, 445−450.
(57) Yang, Q.; Sun, P. Z.; Fumagalli, L.; Stebunov, Y. V.; Haigh, S. J.; Zhou, Z. W.; Grigorieva, I. V.; Wang, F. C.; Geim, A. K. Capillary Condensation under Atomic-Scale Confinement. *Nature* **2020**, *588*, 250−253.
(58) Daian, J. F. Condensation and isothermal water transfer in cement mortar Part I ? Pore size distribution, equilibrium water condensation and imbibition. *Transp. Porous Media* **1988**, *3*, 563−589.
(59) Bradley, R. S.Polymer adsorbed films. Part I. The adsorption of argon on salt crystals at low temperatures and the determinations of surface fields. Part II. The general theory of the condensation of vapours on finely divided solids. *J. Chem. Soc.***1936**. Part I 1467−1474 and Part II 1799−1804.
(60) Yi, J.; Akkutlu, I. Y.; Karacan, C. Ö.; Clarkson, C. R. Gas Sorption and Transport in Coals: A Poroelastic Medium Approach. *Int. J. Coal Geol.* **2009**, *77*, 137−144.
(61) Zhao, W.; Cheng, Y.; Pan, Z.; Wang, K.; Liu, S. Gas Diffusion in Coal Particles: A Review of Mathematical Models and Their Applications. *Fuel* **2019**, *252*, 77−100.
(62) Yang, Y.; Liu, S. Estimation and Modeling of Pressure-Dependent Gas Diffusion Coefficient for Coal: A Fractal Theory-Based Approach. *Fuel* **2019**, *253*, 588−606.
(63) Chen, Y.; Mastalerz, M.; Schimmelmann, A. Characterization of Chemical Functional Groups in Macerals across Different Coal Ranks via Micro-FTIR Spectroscopy. *Int. J. Coal Geol.* **2012**, *104*, 22−33.
(64) Vishnyakov, A.; Ravikovitch, P. I.; Neimark, A. V. Molecular Level Models for CO2 Sorption in Nanopores. *Langmuir* **1999**, *15*, 8736−8742.
(65) Gregg, S. J.; Sing, K. S. W.*Adsorption Surface Area and Porosity*, 2nd Edition; Academic Press, London, 1982.
(66) Sang, G.; Liu, S.; Elsworth, D. Water Vapor Sorption Properties of Illinois Shales Under Dynamic Water Vapor Conditions: Experimentation and Modeling. *Water Resour. Res.* **2019**, *55*, 7212−7228.
(67) Liu, J.; Chen, Z.; Elsworth, D.; Qu, H.; Chen, D. Interactions of multiple processes during CBM extraction: A critical review. *Int. J. Coal Geol.* **2011**, *87*, 175−189.
(68) Charrière, D.; Behra, P. Water Sorption on Coals. *J. Colloid Interface Sci.* **2010**, *344*, 460−467.
(69) Tang, G. H.; Lu, Y. B. A Resistance Model for Newtonian and Power-Law Non-Newtonian Fluid Transport in Porous Media. *Transp. Porous Media* **2014**, *104*, 435−449.
(70) Suuberg, E. M.; Otake, Y.; Yun, Y.; Deevi, S. C. Role of Moisture in Coal Structure and the Effects of Drying upon the Accessibility of Coal Structure. *Energy Fuel.* **1993**, *7*, 384−392.
(71) Gor, G. Y.; Huber, P.; Bernstein, N. Adsorption-induced deformation of nanoporous materials-A review. *Appl. Phys. Rev.* **2017**, *4*, 011303.
(72) Deevi, S. C.; Suuberg, E. M. Physical Changes Accompanying Drying of Western US Lignites. *Fuel* **1987**, *66*, 454−460.
(73) Suuberg, E. M.; Otake, Y.; Langner, M. J.; Leung, K. T.; Milosavljevic, I. Coal Macromolecular Network Structure Analysis: Solvent Swelling Thermodynamics and Its Implications. *Energy Fuel.* **1994**, *8*, 1247−1262.
(74) Sang, G.; Liu, S.; Elsworth, D.; Yang, Y.; Fan, L. Evaluation and Modeling of Water Vapor Sorption and Transport in Nanoporous Shale. *Int. J. Coal Geol.* **2020**, *228*, 103553.
(75) Schmitt, L.; Forsans, T.; Santarelli, F. J. Shale Testing and Capillary Phenomena. *Int. J. Rock Mech. Min. Sci.* **1994**, *31*, 411−427.

https://doi.org/10.1021/acs.langmuir.2c02701
Langmuir 2022, 38, 14941−14958